Multi-Year Observations of Fluorescence and Backscatter at the Southern Ocean Time Series (SOTS) Shed Light on Two Distinct Seasonal Bio-Optical Regimes

Christina Schallenberg[1]*[†], James W. Harley[1], Peter Jansen[1,2], Diana M. Davies[1,2] and Thomas W. Trull[1,2]

[1] Antarctic Climate and Ecosystems Cooperative Research Centre, Hobart, TAS, Australia, [2] Commonwealth Scientific and Industrial Research Organisation Oceans and Atmosphere, Hobart, TAS, Australia

This work presents insights from 6 years of chlorophyll-a (Chl) fluorescence and backscatter (700 nm) data at the Southern Ocean Time Series (SOTS) moorings, located in the Subantarctic Zone (SAZ) southwest of Tasmania. Using local calibrations from available voyage data, the fluorescence and backscatter records were related to Chl and particulate organic carbon (POC), allowing us to estimate and interpret carbon:Chl ratios. Surprisingly, observed carbon:Chl ratios were higher in winter than in summer, indicating that photo-acclimation of phytoplankton to decreased light levels in the deep winter mixed layer is not the main signal. Instead, the data suggest a seasonal succession of two trophodynamic regimes at SOTS: a phytoplankton-dominated community in summer, while in winter the proportion of "non-phytoplankton" POC increases. The two regimes can also be differentiated in an optical index based on fluorescence and backscatter, indicating two distinct bio-optical populations. Seasonal iron limitation and deep winter mixing in the SAZ, reaching as deep as 600 m, likely play key roles in setting the stage for the observed ecological succession of the two trophodynamic regimes.

Keywords: chlorophyll fluorescence, backscatter, SAZ, POC, optical index, Southern Ocean, time series, SOTS

INTRODUCTION

The Subantarctic Zone (SAZ) plays an important role for the marine biological carbon pump because it lies at the interface between two contrasting regions: the nutrient rich polar seas to the south and the nutrient poor subtropical gyres to the north. Indeed, changes in the efficiency of its nutrient consumption appear to have modulated atmospheric CO_2 levels on glacial/interglacial timescales (Sigman and Boyle, 2000). In the present day, the efficiency of this pump affects ocean productivity outside the Southern Ocean via the control of nutrient delivery in the upper limb of the overturning circulation (Sarmiento et al., 2004).

The SAZ is characterized by both iron and light limitation (Sedwick et al., 1999; Boyd et al., 2001). Deposition of aerosols can relieve iron limitation in summer, while deep mixing and Ekman transport provide an initial winter reserve of iron (Ellwood et al., 2008; Bowie et al., 2009).

Nearly complete silicic acid depletion occurs in surface waters in summer (Bowie et al., 2011a,b), potentially influencing phytoplankton community composition, although nitrate concentrations remain high (Lourey and Trull, 2001).

Even though biomass accumulation in the SAZ is only moderate [chlorophyll-a concentrations rarely exceed 1 mg m^{-3} and are generally less than 0.6 mg m^{-3} (Trull et al., 2001; Mongin et al., 2011; Eriksen et al., 2018)], annual Net Community Production (NCP; Weeding and Trull, 2014) and associated CO_2 drawdown (Shadwick et al., 2015) are similar to those of North Atlantic waters where a strong spring bloom occurs with chlorophyll-a concentrations exceeding 3 mg m^{-3} (Shadwick et al., 2011). The longer duration of CO_2 drawdown in the SAZ appears to be a likely driver of this unexpectedly strong biological pump contribution, but little is yet known regarding its seasonal controls, especially in winter for which observations are very sparse. The Southern Ocean Time Series (SOTS) autonomous observatory offers the only multi-year full-annual observations to examine this issue.

The SOTS (**Figure 1**) is located north of the Subantarctic Front that marks the northern edge of the Antarctic Circumpolar Current. The moorings are in deep waters (>4500 m) west of the Tasman Rise, and the site exhibits oceanographic properties representative of the Australian sector of the SAZ (from $\sim$90 to 145°E; Trull et al., 2001). Waters flowing southward in the East Australian Current occasionally reach this region by transiting through channels in the Tasman Rise (Herraiz-Borreguero and Rintoul, 2011).

Since 2009, optical sensors measuring backscatter (at 700 nm) and chlorophyll fluorescence have been deployed on two different mooring designs at SOTS. These sensors provide year-round data and allow insights into the seasonal evolution of biomass accumulation at the site. While chlorophyll fluorescence is specific to phytoplankton (Lorenzen, 1966; Roesler et al., 2017), particulate backscatter (b_{bp}) is less discerning and can include a signal from zooplankton, detritus, bacteria, bubbles, and lithogenic material (Morel and Ahn, 1991; Stramski and Kiefer, 1991; Ahn et al., 1992; Terrill et al., 2001). However, there tends to be a strong relationship between b_{bp} and particulate organic carbon (POC) as measured on discrete samples (e.g., Stramski et al., 1999; Cetinic et al., 2012), even if the debate continues on whether this relationship mainly reflects backscattering by organic particles themselves, for example as could be explained by violation of Mie scattering assumptions (Whitmire et al., 2010; Organelli et al., 2018), or whether it is the result of backscattering by co-varying quantities (e.g., Zhang et al., 2011). In contrast, fluorescence (FChl, see **Table 1**) does not always show a linear relationship with chlorophyll-a (Chl) due to non-photochemical quenching, which decreases fluorescence relative to Chl under supersaturating light conditions (Cullen and Lewis, 1995; Xing et al., 2012).

To the first degree, optical properties of a water mass, including b_{bp}, covary with Chl concentration, a concept widely known as the "bio-optical assumption" (Smith and Baker, 1978; Siegel et al., 2005). However, deviations from this simple relationship are widely observed in the global ocean, and indeed may hold additional information about particle size distribution
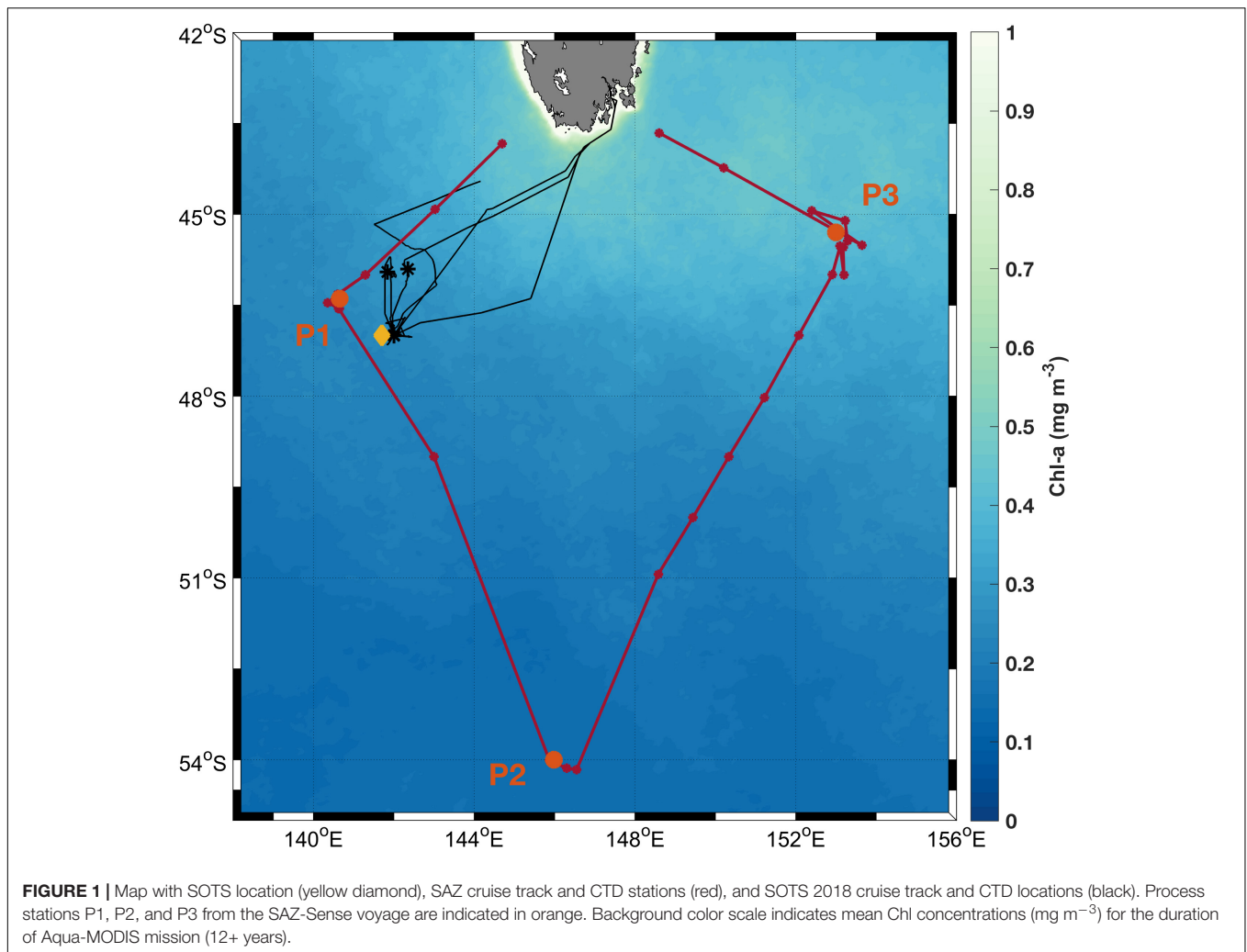
TABLE 1 | Nomenclature used.

Name	Unit	How measured
Chl	mg m^{-3}	Chl as measured by HPLC on filters; discrete measurements on samples from SAZ-Sense cruise
FChl	mg m^{-3}	Fluorescence measured by an optical instrument; manufacturer's Chl calibration, hence the units; *treated as Fluorescence*
Chl-F	mg m^{-3}	Chl estimated from a fluorescence sensor based on our local calibration for SOTS (using SAZ-Sense Chl data; see section "Calibration Against POC and Pigment Data From SAZ-Sense Voyage")
POC	mg m^{-3}	Particulate organic carbon; discrete measurement on filters from SAZ-Sense cruise
b_{bp}	m^{-1}	Particulate backscattering, measured with an optical instrument and calibrated according to manufacturer's instructions; seawater contribution subtracted (see section "Factory Calibrations")
c_p	m^{-1}	Particulate attenuation, measured with an optical instrument; seawater contribution subtracted from total beam attenuation (see section "Establishing a Relationship Between Beam c_p and b_{bp}")
POC_b_{bp}	mg m^{-3}	POC estimated from optical measurements of b_{bp} using local calibration from SAZ-Sense voyage (includes c_p-b_{bp} conversion, see sections "Establishing a Relationship Between Beam c_p and b_{bp}" and "Calibration Against POC and Pigment Data From SAZ-Sense Voyage")
C_{phyto}_b_{bp}	mg m^{-3}	Phytoplankton carbon estimated from b_{bp} using Graff et al. (2015) relationship, via Haentjens et al. (2017) conversion

and phytoplankton community structure (e.g., Vaillancourt et al., 2004; Whitmire et al., 2010; Cetinic et al., 2015; Lacour et al., 2017). An optical index based on the FChl:b_{bp} ratio has been used as a proxy for diatom dominance, for example in the North Atlantic (Cetinic et al., 2015; Lacour et al., 2017), and the global variability of this index based on float data has been characterized by Barbieux et al. (2018). When local calibrations are used, the ratio between derived POC and Chl may be a proxy for the carbon:Chl (C:Chl) ratio of the resident phytoplankton, which in turn is related to their photo-acclimation and nutritional status (Geider, 1987; Falkowski and LaRoche, 1991; Greene et al., 1992; Smith and Kaufman, 2018).

The 6-year record of fluorescence and backscatter from the SOTS mooring thus holds the promise to reveal information about a number of attributes of the resident microorganisms, and to track their evolution throughout the year. Specifically, we set out to test the following hypotheses:

1. Light acclimation dominates the C:Chl ratio as estimated based on the optical proxies. Low light in winter should lead to increased Chl production per cell, hence the expected trend would be decreased C:Chl ratios in winter.
2. Ecosystem structure (trophodynamics) is the dominant driver, with increased proportions of detritus and bacteria in winter, while phytoplankton dominate in summer. Increased POC (and b_{bp}) relative to Chl (and FChl) would be expected in winter due to smaller cell sizes among

FIGURE 1 | Map with SOTS location (yellow diamond), SAZ cruise track and CTD stations (red), and SOTS 2018 cruise track and CTD locations (black). Process stations P1, P2, and P3 from the SAZ-Sense voyage are indicated in orange. Background color scale indicates mean Chl concentrations (mg m^{-3}) for the duration of Aqua-MODIS mission (12+ years).

all fractions (phytoplankton, detritus, bacteria) and less investment in Chl.

3. Phytoplankton community structure (floristics) drives the signal: Diatoms dominate in summer and show increased fluorescence relative to b_{bp} as per the "optical community index" introduced by Cetinic et al. (2015) and Lacour et al. (2017). An increase in the FChl:b_{bp} ratio would be expected in summer.

In what follows we make a clear distinction between two important ratios:

I The C:Chl ratio expressed as either POC:Chl-F or C_{phyto}:Chl-F (see **Table 1**), which employs regional calibrations of the fluorescence and backscatter sensors.

II The "optical community index" (FChl:b_{bp}), which does not employ any regional calibrations but relies solely on manufacturer's calibrations.

Although related to each other, the two formulations hold different kinds of information and allow us to compare to different data sets. A long history of measured C:Chl ratios allows us to compare our data to satellite, *in situ* and laboratory measurements made over decades. The FChl:b_{bp} ratio on the other hand explicitly includes the possibility that the fluorescence:Chl ratio can be variable (e.g., Proctor and Roesler, 2010; Roesler et al., 2017) and thus does not try to "correct" for this fact. This means that variations in the fluorescence part of the optical community index may include both changes in C:Chl and changes in fluorescence:Chl.

MATERIALS AND METHODS

SOTS Mooring Data

The SOTS Observatory located at 140°E and 47°S provides high temporal resolution observations in Subantarctic waters. It is located north of the Polar Front and falls into the Subantarctic Province as defined by Longhurst (2007). This area of the Southern Ocean is biogeochemically distinct from the Southern Ocean provinces further south, namely the Antarctic Province and the Austral Polar Province (Longhurst, 2007; Vichi et al., 2011).

The SOTS site southwest of Tasmania is comprised of a number of elements including a deep ocean sediment trap mooring (SAZ), a surface biogeochemistry mooring (Pulse) and an air–sea flux mooring (SOFS). Located in the SAZ, the site is particularly vulnerable to the extreme weather events that typify the area including very large waves, strong currents and severe storms, presenting significant technical and engineering challenges (Trull et al., 2010).

Four different Wetlabs FLNTUS instruments, measuring Chl fluorescence (FChl, see **Table 1** for a full list of terms used in this manuscript) and backscattering at 700 nm (for a scattering angle of 140°), were deployed at SOTS between 2009 and 2016, on two different mooring designs. Instruments on the Pulse mooring were deployed at 30 m depth, in a downward looking configuration mounted on the bottom plate of the Remote Area water Sampler and instrument package. Instruments on the SOFS moorings were mounted on the base of the 2.7 m diameter meteorological surface float, at ∼0.5 m depth, also in a downward looking configuration. All sensors had an integral "bio-wiper," which rotated a plastic wiper past the sensing window prior to measurement. In addition, copper metal sheet was added surrounding the instruments to further discourage bio-fouling (beginning in 2012). Nonetheless, some bio-fouling did occur, especially the growth of gooseneck barnacles which hung within the sensor view. All data have undergone rigorous quality control (Schallenberg et al., 2019), and only data flagged as "good" (i.e., QC flag <2) were used in this analysis. Furthermore, to avoid any bias from non-photochemical quenching, only night-time data were used.

Factory Calibrations

All backscatter and fluorescence data from the FLNTUS instruments were calibrated using factory-supplied dark values and scale factors, yielding FChl in units of mg m^{-3} and backscatter on a turbidity scale (NTU). The latter was converted to scattering in the backward direction, $\beta(140°)$, at 700 nm based on a conversion factor supplied by Wetlabs:

$$\beta(140°)(m^{-1}sr^{-1}) = \text{turb} \times 0.002727$$

The particulate backscattering coefficient was then calculated as follows, with the scattering of seawater and salts, $\beta(140°)_{sw}$ derived following Zhang et al. (2009), and $\chi_P = 1.17$ sr for a scattering angle of 140° (Sullivan and Twardowski, 2009):

$$b_{bp}(m^{-1}) = 2 \times \pi \times \chi_p \times (\beta(140°) - \beta(140°)_{sw})$$

Data Quality

Despite the rigorous QC, we found that during winter, backscatter measurements collected near the surface were much higher than those collected at 30 m depth (**Figure 2A**). No such difference was observed between Chlorophyll fluorescence measurements (**Figure 2B**). We suspect that the high winter backscatter values at the surface are due to bubble injection from breaking waves during the stormy winter season (e.g., Zhang et al., 1998; Terrill et al., 2001). As a result, data from the surface moorings were not used in any subsequent analyses.

Voyage Data
SAZ-Sense Voyage 2007
The SAZ-Sense (Sensitivity of the SAZ to environmental change) expedition sampled a diamond-shaped area south of Tasmania in austral summer of 2007 (**Figure 1**). Details of the oceanographic setting and sampling are described by Bowie et al. (2011a). Pigment (high performance liquid chromatography, HPLC) and POC samples were taken at 26 CTD stations. Treatment and analysis of samples have been described elsewhere (de Salas et al., 2011; Cassar et al., 2015). A Wetlabs CStar transmissometer and Wetlabs ECO-Fl fluorometer were mounted on the CTD rosette and calibrated according to factory specifications. In order to prevent non-photochemical quenching from affecting results involving FChl, only fluorescence data collected at night or at a depth of greater than 25 m were used in this study.

SOTS Voyage 2018
The SOTS voyage to the mooring site took place aboard the RV Investigator in March 2018 (**Figure 1**). The voyage comprised six deployments of the CTD-Rosette system to depths ranging from 500 to 2250 m, with both a Wetlabs CStar beam transmissometer and a Wetlabs FLBBRTD backscatter sensor mounted on the frame simultaneously. Data from these optical sensors was binned to 1 m depth resolution.

Regional Calibrations

Using data from the SAZ-Sense voyage in 2007 and the SOTS voyage in 2018, we established conversion factors from optical measurements of fluorescence chlorophyll, FChl, and particulate backscatter, b_{bp}, to Chl-F (mg m^{-3}) and POC-b_{bp} (mg m^{-3}), respectively. Due to a mismatch in sensors, i.e., the POC data on the SAZ-Sense voyage was matched with a beam transmissometer rather than a backscatter sensor, we also had to convert particulate beam transmission (c_p) to b_{bp}. This was accomplished using data from the SOTS voyage in March 2018, when both a beam transmissometer and a backscatter sensor were mounted on the CTD.

Establishing a Relationship Between Beam c_p and b_{bp}
The optical sensor output from the Wetlabs CStar beam transmissometer (25 cm path length) on the SOTS voyage was delivered in units of percent, while the backscattering sensor on the Wetlabs FLBBRTD delivered scattering in the backward direction at a single angle, $\beta(140°)$, at 700 nm (sr^{-1} m^{-1}). These entities were transformed into particle attenuation (c_p) and particulate backscatter (b_{bp}) as follows.
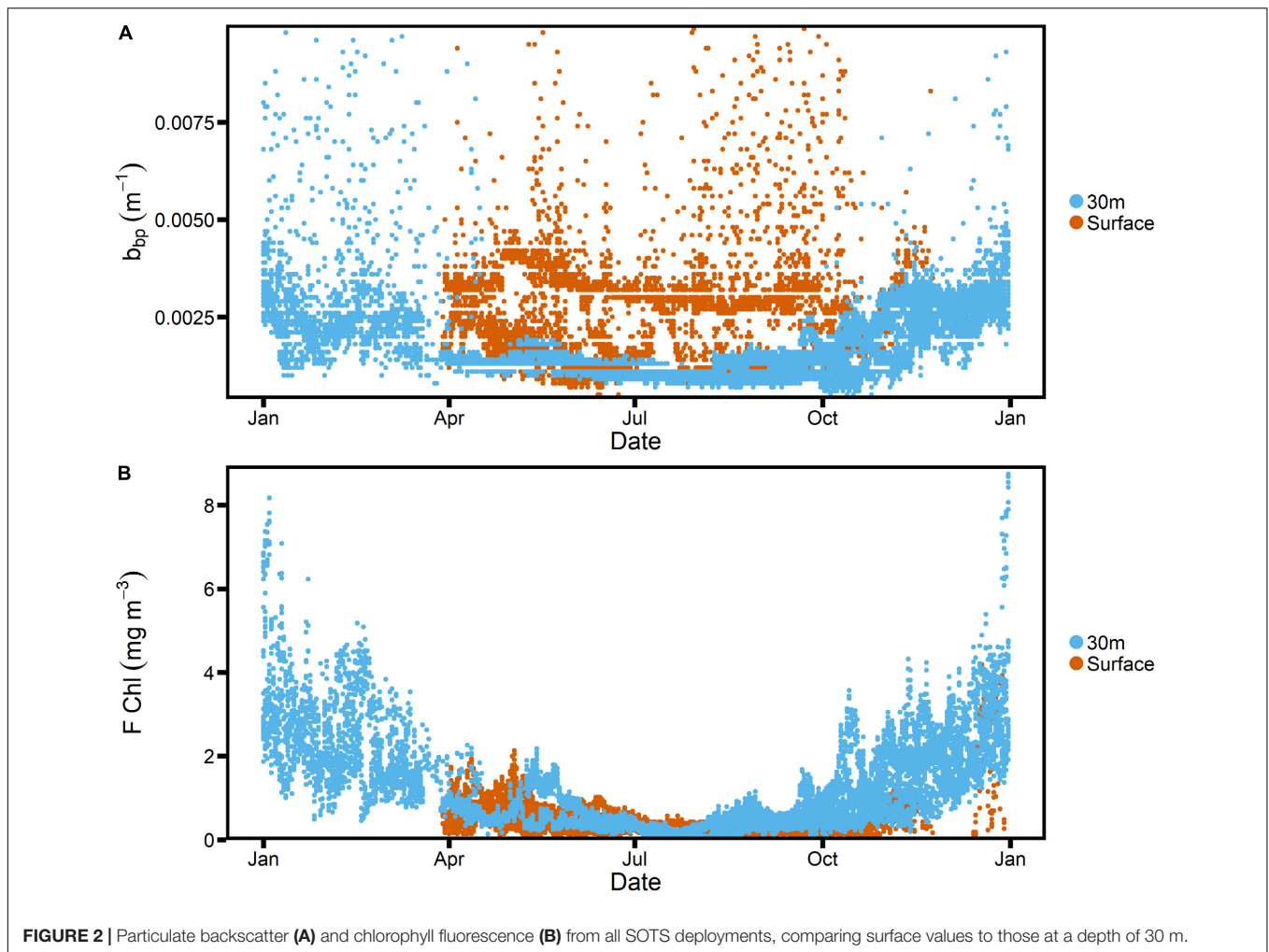
Total beam attenuation (c) can be calculated from % transmissivity:

$$c(m^{-1}) = -\frac{1}{0.25\ m} \times \text{logn}\left(\frac{\text{transmissometer (\%)}}{100}\right),$$

where 0.25 m refer to the path length of the instrument.

To convert total beam attenuation to particulate attenuation (c_p), the contribution by seawater (c_{sw}) needs to be subtracted:

$$c_p = c - c_{sw}$$

FIGURE 2 | Particulate backscatter **(A)** and chlorophyll fluorescence **(B)** from all SOTS deployments, comparing surface values to those at a depth of 30 m.

In this study, c_{sw} was derived from measurements of c at 1000 m depth, where particle concentrations can be assumed to be negligible.

The particulate backscattering was calculated from $\beta(140°)$ as described above (section "Factory Calibrations"). To derive the relationship between c_p and b_{bp} on the SOTS voyage, only data from shallower than 150 m were used (surface data not excluded because no bias due to bubbles was apparent), and the resulting relationship was as follows ($r^2 = 0.95$, $n = 653$, **Figure 3**):

$$b_{bp}(700) = 0.00345 \times c_p^{0.449}$$

Calibration Against POC and Pigment Data From SAZ-Sense Voyage

The respective local calibrations were achieved using linear regression (**Figure 4**), with the following relationships:
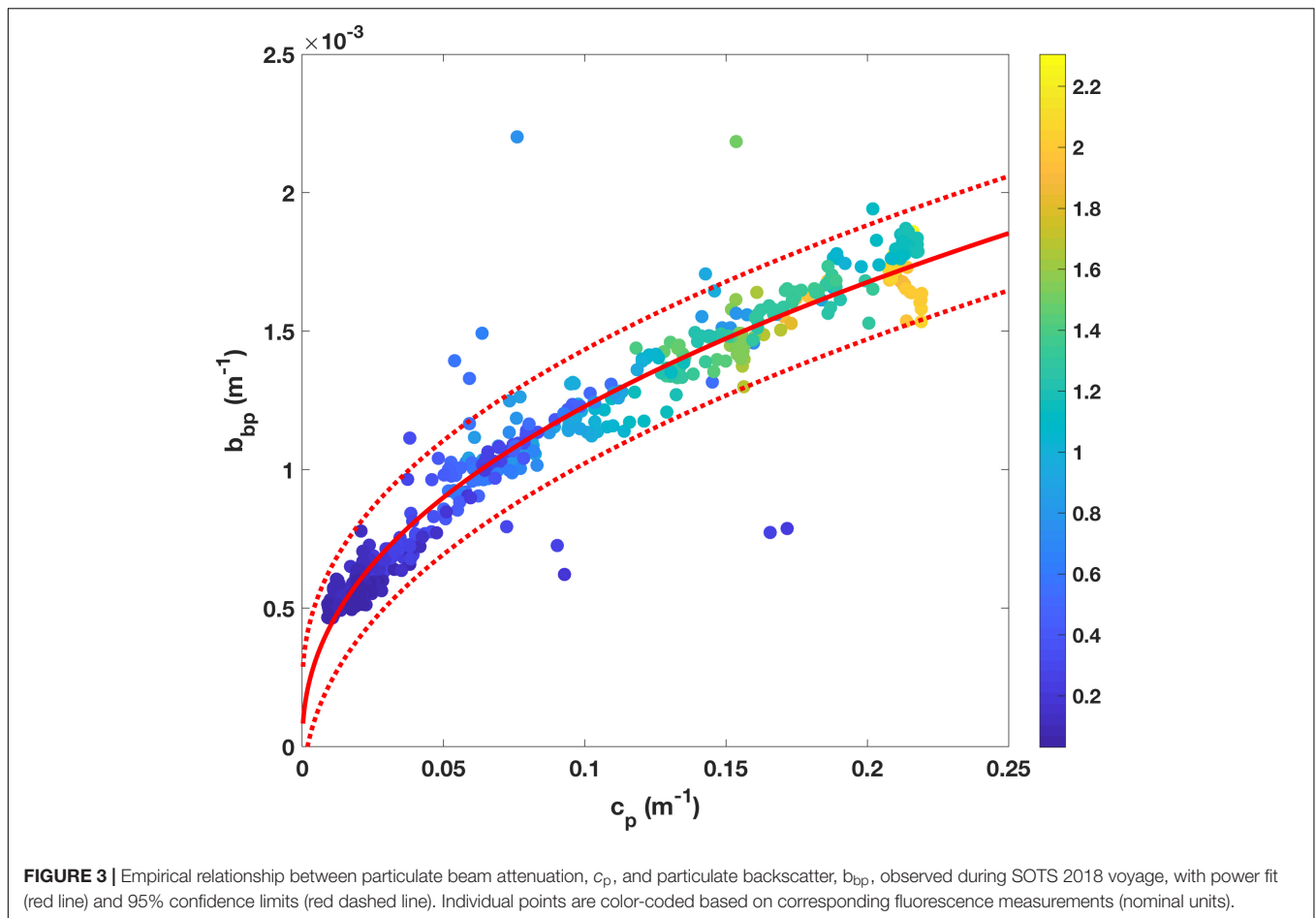
$$Chl = 0.320 \times FChl \quad r^2 = 0.79, \ p \ll 0.01, \ n = 227$$

$$POC = 37601 \times b_{bp} + 4.95 \quad r^2 = 0.37, \ p \ll 0.01, \ n = 108$$

Only the Chl regression was forced through the origin for easy comparison with the "slope factor" determined by

Roesler et al. (2017) and reflecting the fact there should be little FChl in the absence of Chl (but see Xing et al., 2016), whereas there can be significant backscatter in the absence of POC, for example from biogenic frustules and lithogenic minerals. While robust regression lines, i.e., fitted with a regression that puts reduced weight on presumed outliers so they have a smaller impact on the fitted regression line (Maronna and Yohai, 2000), are shown for comparison, we decided to use the regular regressions for the following reasons: for the Chl-F calibration, we know that the large scatter is not the result of outliers but of different phytoplankton communities encountered in different regions of the voyage (see **Figure 5A**), and due to frontal movements and the passage of mesoscale eddies, all of these communities may be present at SOTS during different times of the year. Hence we also decided to use a regression that includes all the data. The POC calibration shows no clear regional differences (**Figure 5B**), and the robust and regular regression lines fall very close together. For consistency and in order to report a regression coefficient r^2, we thus used the regular linear regression for our calibration in both cases.

The relationship between FChl and Chl (**Figure 4A**) is known to show strong regionality, with up to 7-fold variation globally

FIGURE 3 | Empirical relationship between particulate beam attenuation, c_p, and particulate backscatter, b_{bp}, observed during SOTS 2018 voyage, with power fit (red line) and 95% confidence limits (red dashed line). Individual points are color-coded based on corresponding fluorescence measurements (nominal units).

and the largest divergence from manufacturer's calibrations observed in the Southern Ocean (Roesler et al., 2017). We found a slope of $1/0.32 = 3.12$, which is slightly below the slope of 3.46 for the South Indian Ocean reported by Roesler et al. (2017). Comparing FChl data from the SOTS mooring to satellite Chl observations, Eriksen et al. (2018) found good agreement when a slope of 4 was assumed, which is similar to the regional calibration for the Atlantic SO as reported by Thomalla et al. (2017). Our slope thus falls on the low end of expectations, making it more likely that Chl will be overestimated than underestimated.

Figure 4B shows the relationship between b_{bp} and POC, derived using the SAZ-Sense data, with the addition of 4 published relationships for different Southern Ocean regions (Stramski et al., 1999; Haentjens et al., 2017; Rembauville et al., 2017). We note that our regressions agree well with 3 out of 4 of the published relationships, instilling confidence that our c_p-b_{bp} conversion is robust.

Smoothing of Annual Cycles With a General Additive Model

A generalized additive model (GAM) was used to create smoothed lines from the data shown in several figures, preserving the overall trend of the seasonal cycle. The line produced by the
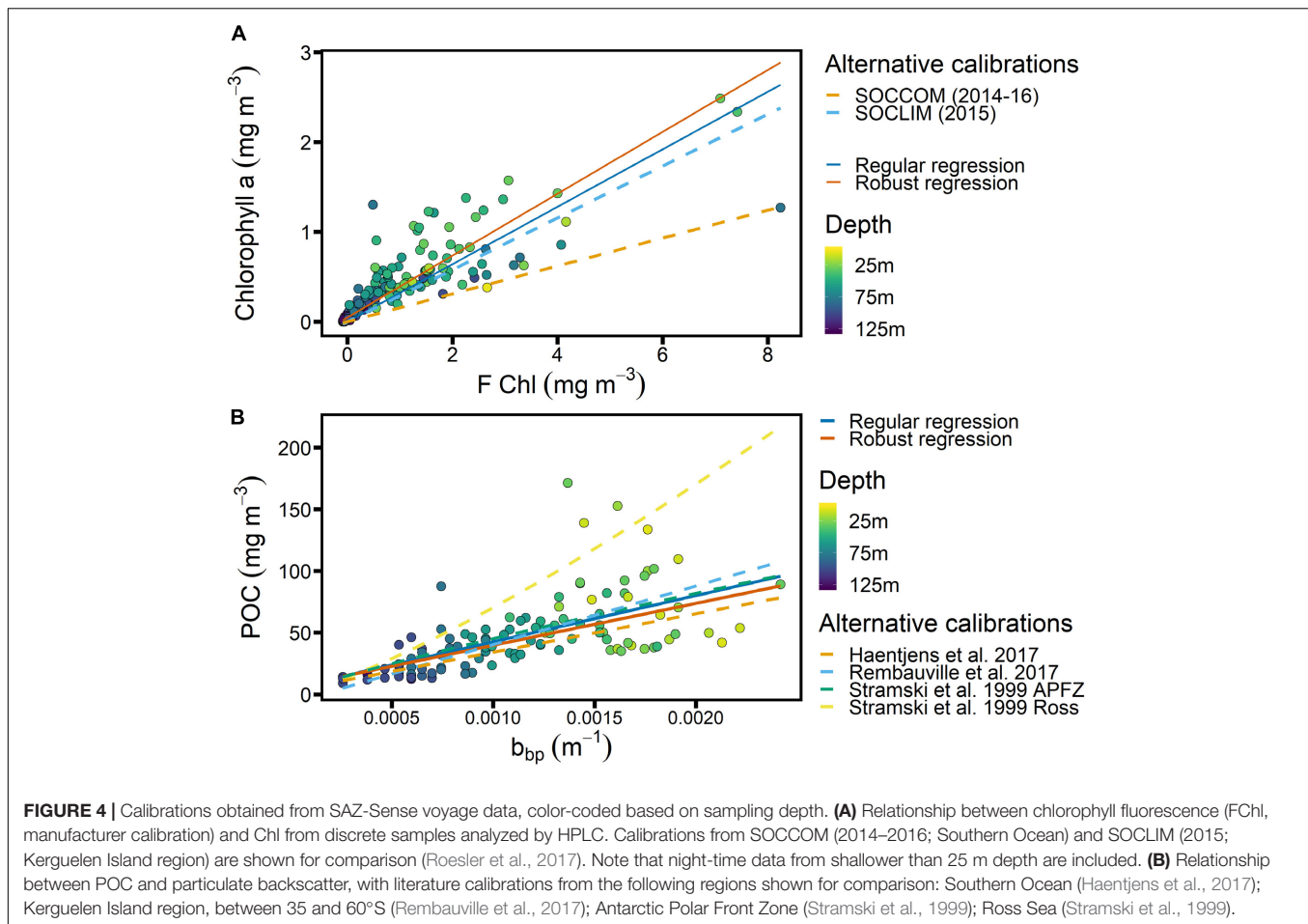
GAM is a sum of smooth functions relating the response variable to the predictor variable (Wood, 2001). This type of modeling is useful for the identification of long-term trends in time series data (e.g., Bellido et al., 2001; Underwood, 2009). In all figures where this model is presented, a cubic regression spline was used as the smoothing basis. The number of basis dimensions for each model was decided upon using the *gam.check*() function from the "mgcv" R package.

RESULTS AND DISCUSSION

We explore 6 years of SOTS data to evaluate the hypotheses regarding drivers of bio-optical signatures that were put forward in the introduction. However, we first examine our data for biases that may have been introduced with the respective calibrations.

Potential Seasonal Biases of Calibrations

As mentioned above, we adopted a constant Chl-F calibration for the full seasonal cycle, thus not accounting for possible fluctuations in the FChl:Chl ratio throughout the year such as could be caused by changes in phytoplankton community structure and/or nutrient limitation (Behrenfeld et al., 2009; Proctor and Roesler, 2010; Roesler et al., 2017). Indeed, seasonal

FIGURE 4 | Calibrations obtained from SAZ-Sense voyage data, color-coded based on sampling depth. **(A)** Relationship between chlorophyll fluorescence (FChl, manufacturer calibration) and Chl from discrete samples analyzed by HPLC. Calibrations from SOCCOM (2014–2016; Southern Ocean) and SOCLIM (2015; Kerguelen Island region) are shown for comparison (Roesler et al., 2017). Note that night-time data from shallower than 25 m depth are included. **(B)** Relationship between POC and particulate backscatter, with literature calibrations from the following regions shown for comparison: Southern Ocean (Haentjens et al., 2017); Kerguelen Island region, between 35 and 60°S (Rembauville et al., 2017); Antarctic Polar Front Zone (Stramski et al., 1999); Ross Sea (Stramski et al., 1999).
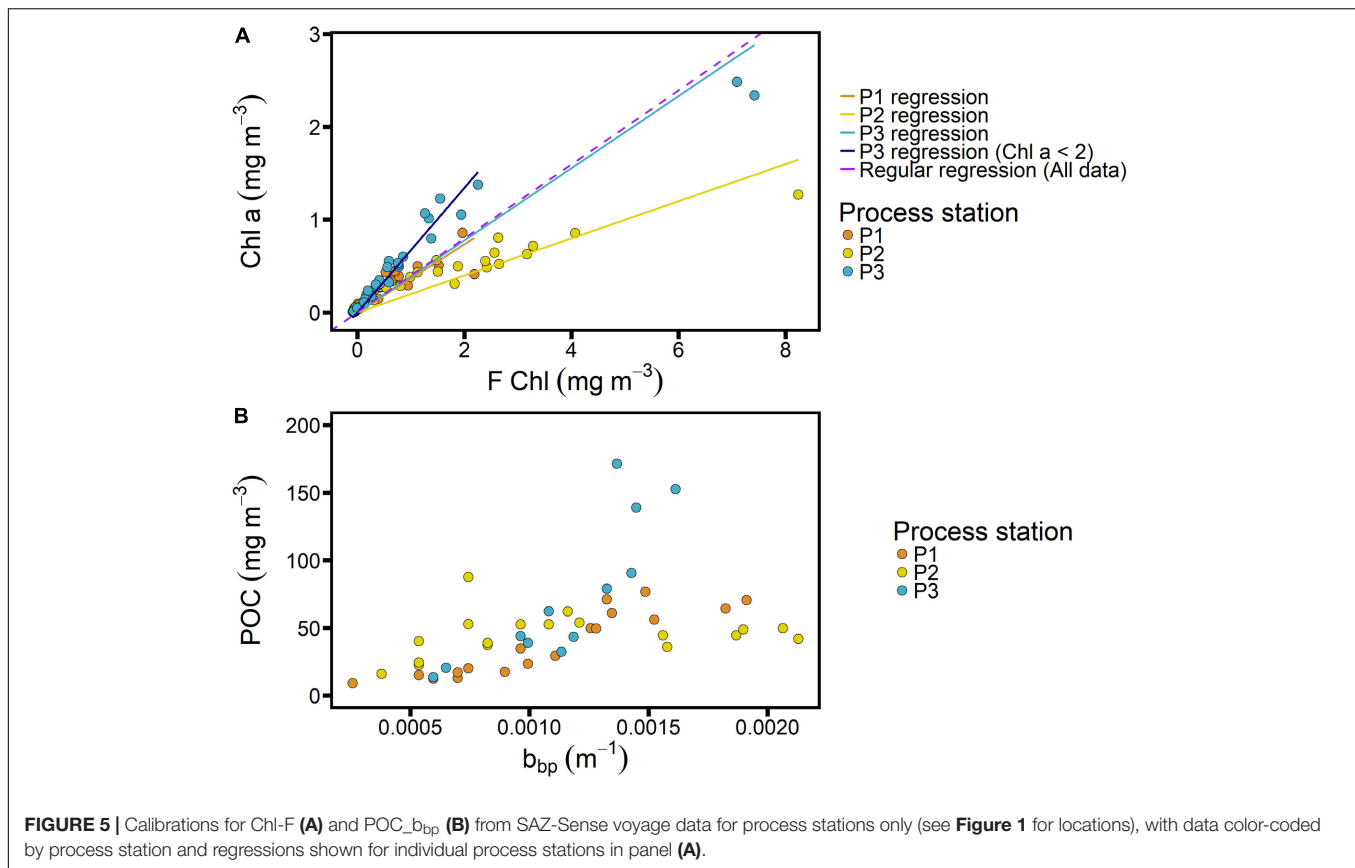
variation is expected. With respect to community composition in the SAZ-Sense cruise data, we can assume that the polar region (P2 in **Figure 5**) is representative of a spring community at SOTS, while the subtropical region (P3) may represent SOTS in the fall. The regression for P3 excluding the two highest points yields a slope of 1.5 (**Figure 5A**), which is lower than the factor 2.3 reported by Trull et al. (2019) for samples taken in March at the SOTS site, but it diverges in the same direction from the average slope of 3.12. This would suggest that overall, our calibration overestimates Chl concentrations in spring and underestimates them in the fall.

The estimated Chl concentrations at SOTS are shown in **Figure 6D**, indicating maximum Chl concentrations as high as 2 mg m^{-3} in summer, with the GAM-smoothed time series indicating maximum Chl concentrations just above 1 mg m^{-3} and an annual range comprising more than an order of magnitude. While data to compare these numbers to are sparse, satellite-based estimates by Eriksen et al. (2018) found maximum Chl concentrations at SOTS to be <0.75 mg m^{-3} in the 2010/2011 summer, and Ryan-Keogh et al. (2018) report <1 mg m^{-3} for the SAZ in the Atlantic Ocean. This indicates that our Chl estimates in summer are on the high end relative to what has been reported elsewhere, and are more likely to be overestimates than underestimates.

The biggest caveat, however, is the lack of winter data to constrain calibrations during that season. Using the attenuation of photosynthetically active radiation as a proxy for Chl in the mixed layer (defined based on a temperature threshold of 0.3°C), Trull et al. (2019) estimate that winter concentrations of Chl at SOTS could be as high as 0.2–0.3 mg m^{-3}, which is considerably higher than the winter Chl-F presented in **Figure 6D**, which is as low as ~0.03 mg m^{-3} in July. We cannot exclude the possibility that nutrient effects on the fluorescence:Chl ratio, e.g., decreased fluorescence relative to Chl due to a relief of iron limitation, could be at least partially responsible for this mismatch (e.g., Behrenfeld et al., 2009), thus leading to an underestimate of Chl-F in winter.

The POC-b_{bp} relationship appears less variable than the Chl-F calibration between regions (and thus inferred seasonality in the SAZ; see **Figure 5B**), and our calibration compares well with other relationships developed for the Southern Ocean (**Figures 4B, 6B**). We therefore do not expect large biases from the applied POC_b_{bp} calibration, with the caveat that we are not aware of any winter data to inform calibrations, as is also true for Chl-F. Lastly, we are unable to assess year-to-year variability in calibrations, as might be expected from varying phytoplankton community compositions between years.

With respect to C:Chl ratios, e.g., as can be derived from POC_b_{bp}:Chl-F (see **Figures 6A,B**), the expected seasonal

FIGURE 5 | Calibrations for Chl-F **(A)** and POC_b_{bp} **(B)** from SAZ-Sense voyage data for process stations only (see **Figure 1** for locations), with data color-coded by process station and regressions shown for individual process stations in panel **(A)**.

bias in Chl-F calibrations would lead to an underestimate of POC_b_{bp}:Chl-F ratios in the spring and an overestimate in the fall. An overestimate of Chl-F concentrations in general would underestimate resulting C:Chl ratios.
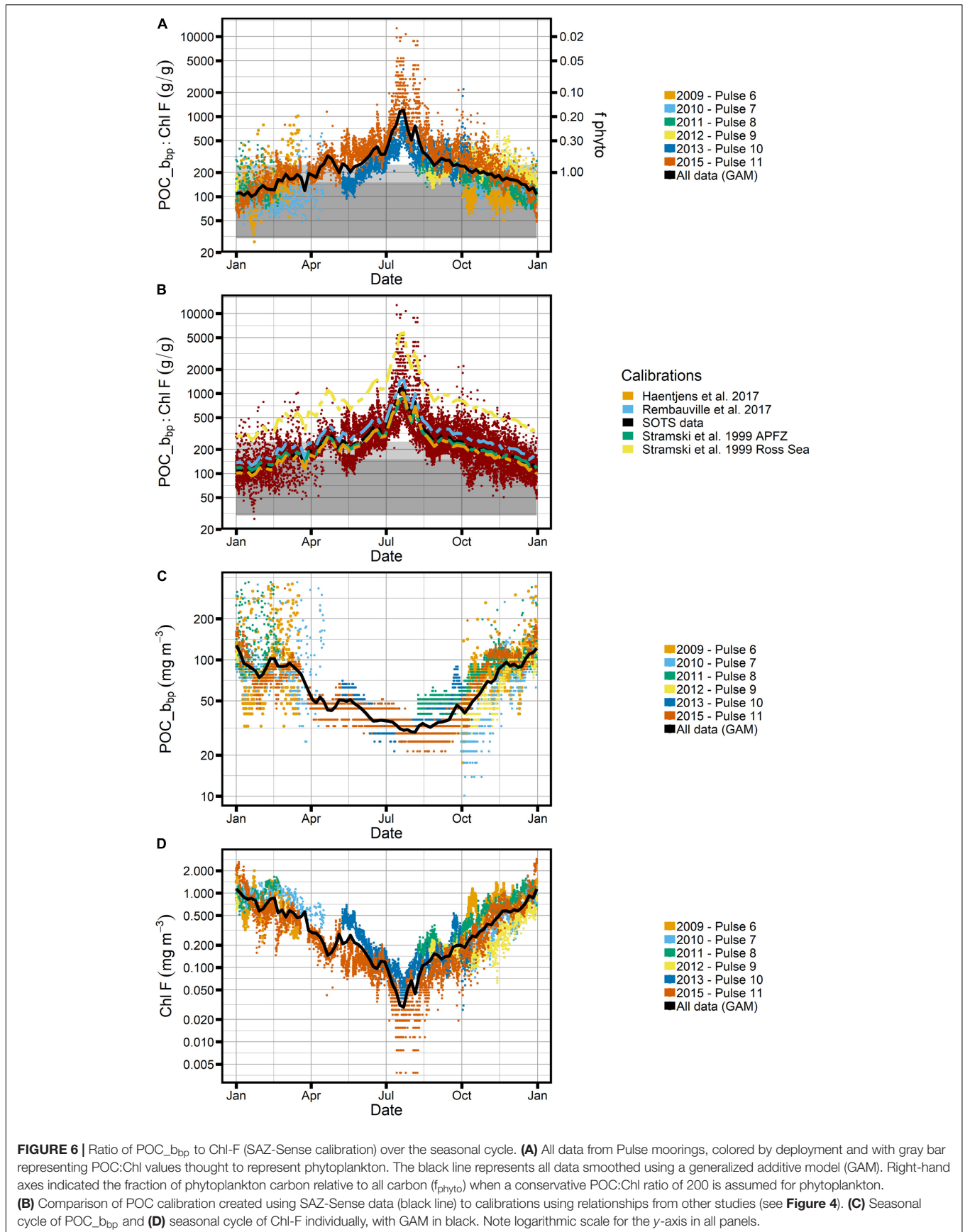
Carbon:Chl Ratios

The POC:Chl ratio is a widely used approximation of the C:Chl ratio. It can readily be measured with established methods and is appropriate under many circumstances, especially when phytoplankton can be assumed to make up a constant fraction of the POC pool, e.g., in laboratory studies. However, this assumption doesn't always hold in the ocean, where phytoplankton have been observed to contribute between 19 and 49% of POC (Behrenfeld et al., 2005 and references therein). Other constituents of the POC pool include detritus, bacteria and zooplankton, and their relative contribution may vary regionally and seasonally.
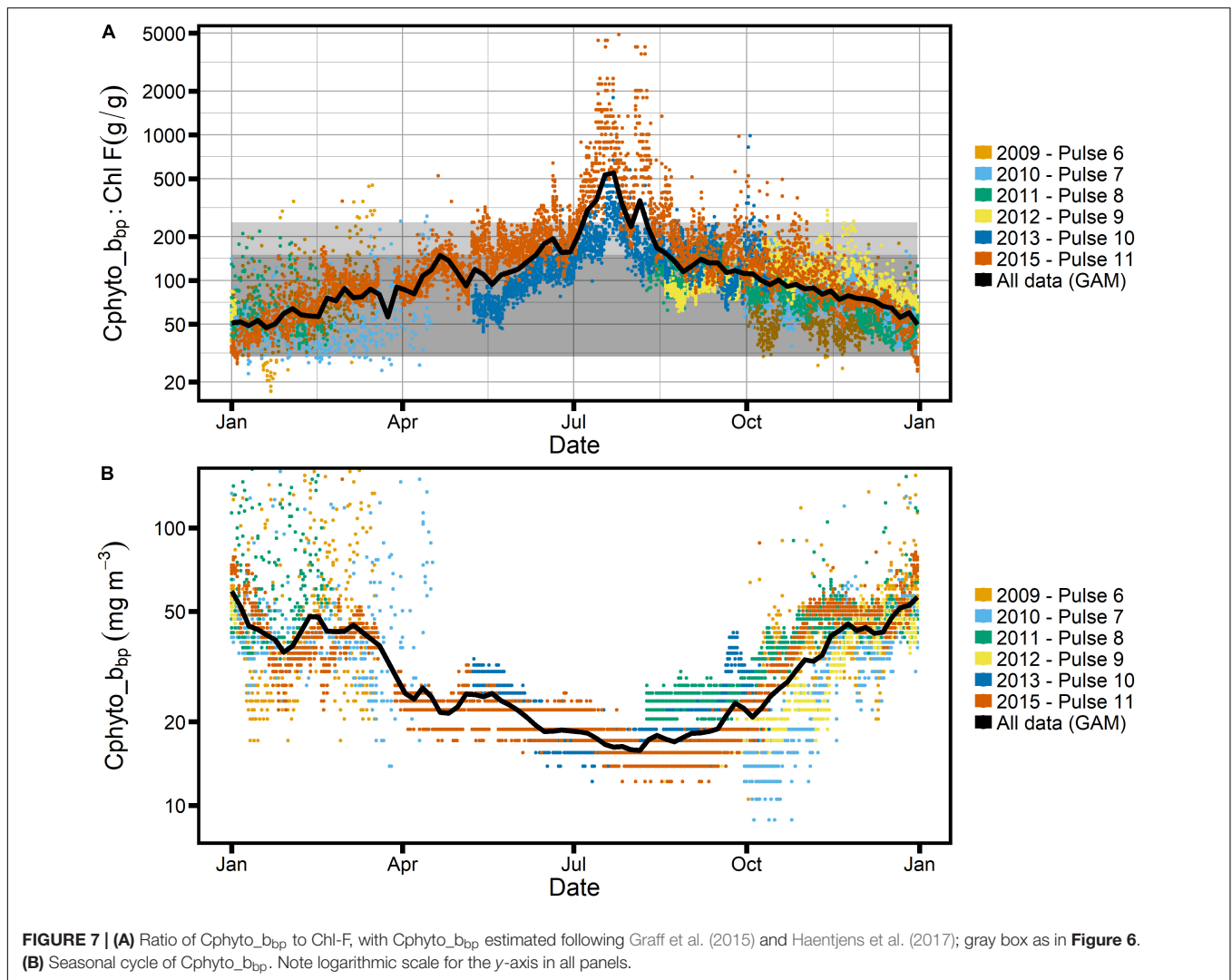
Another complication is that the backscatter signal recorded by the FLNTUS instrument, and hence calibrated against POC, is not specific to phytoplankton. Recent research suggests that the bulk of the backscattering signal measured in the ocean stems from particles larger than 1 μm (Organelli et al., 2018), indicating that phytoplankton would be a large contributor, but detritus and small zooplankton can be of similar particle size. Even so, a linear global ocean relationship has been established between $b_{bp}(470)$ and phytoplankton carbon, C_{phyto}, as estimated using flow-cytometric sorting (Graff et al., 2015).

Following the approach of Haentjens et al. (2017) allowed us to estimate C_{phyto} from $b_{bp}(700)$, presented in **Figure 7**. Most of our data fall within the limits of the Graff et al. (2015) calibration, which was dominated by C_{phyto} values between 5 and 50 mg m^{-3}.

Phytoplankton Light Acclimation

Photo-acclimation is one of the fundamental responses of phytoplankton to changing light fields (e.g., Geider, 1987; Falkowski and LaRoche, 1991), with changes in the C:Chl ratio one of the most readily measured manifestations that is even accessible by satellite (Behrenfeld et al., 2005; Graff et al., 2016; Westberry et al., 2016). Given the stark seasonal changes in incident light and mixed layer depth at the SOTS site, leading to significantly reduced mixed layer light levels in winter compared to summer (**Figure 8**), our first hypothesis was thus that the observed signal in C:Chl ratios is predominantly driven by light acclimation of phytoplankton, with decreased C:Chl ratios expected in winter when light is low. Such annual cycles in the C:Chl ratio have been observed in subarctic environments in the Northern hemisphere, for example in the North Atlantic and Northeast Pacific Oceans (Westberry et al., 2016). However, as **Figures 6A**, **7A** clearly illustrate, the data from 6 years of mooring deployments at the SOTS site paint a different picture and do not support the light acclimation hypothesis. Both the POC_b_{bp}:Chl-F ratio and the C_{phyto}_b_{bp}:Chl-F ratio increase in austral winter, with a peak in

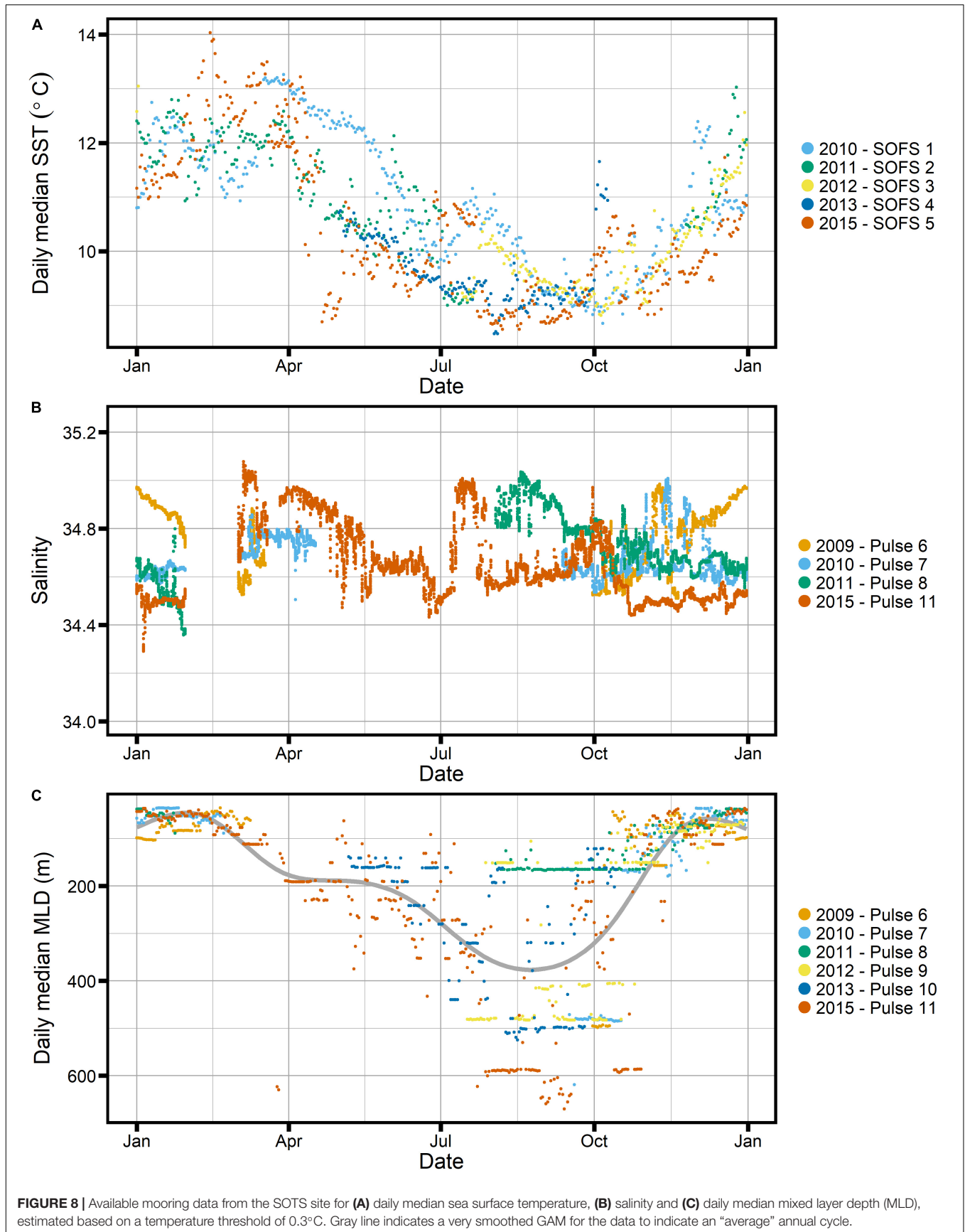**FIGURE 6 |** Ratio of POC_b$_{bp}$ to Chl-F (SAZ-Sense calibration) over the seasonal cycle. **(A)** All data from Pulse moorings, colored by deployment and with gray bar representing POC:Chl values thought to represent phytoplankton. The black line represents all data smoothed using a generalized additive model (GAM). Right-hand axes indicated the fraction of phytoplankton carbon relative to all carbon (f_{phyto}) when a conservative POC:Chl ratio of 200 is assumed for phytoplankton. **(B)** Comparison of POC calibration created using SAZ-Sense data (black line) to calibrations using relationships from other studies (see **Figure 4**). **(C)** Seasonal cycle of POC_b$_{bp}$ and **(D)** seasonal cycle of Chl-F individually, with GAM in black. Note logarithmic scale for the *y*-axis in all panels.

FIGURE 7 | (A) Ratio of Cphyto_b$_{bp}$ to Chl-F, with Cphyto_b$_{bp}$ estimated following Graff et al. (2015) and Haentjens et al. (2017); gray box as in **Figure 6**.
(B) Seasonal cycle of Cphyto_b$_{bp}$. Note logarithmic scale for the *y*-axis in all panels.

July/August. This would indicate an increased C:Chl ratio at the time of year when light is minimal due to deep mixed layers and short solar days.

These results lead us to reject the light acclimation hypothesis, noting that our observations regarding the annual cycle in C:Chl ratios are consistent with glider-based estimates made by Thomalla et al. (2017) for the SAZ in the Atlantic Southern Ocean. Analysing optical data similar to ours, these authors did also observe a seasonal signal in C:Chl that did not appear to be dominated by phytoplankton light acclimation. However, a cautionary note is warranted regarding the conversion of winter fluorescence data to Chl. The FChl:Chl ratio in winter could be significantly different from that in summer, for example as a result of relieved iron limitation after deep mixing and/or resulting from a different phytoplankton community (Roesler et al., 2017). Due to the lack of winter data, the FChl:Chl relationship is poorly constrained in that season – a limitation suffered by both the data presented by Thomalla et al. (2017) and our own data. However, this limitation does not apply to C:Chl ratios derived from satellites (e.g., Behrenfeld et al., 2005; Graff et al., 2016;

Westberry et al., 2016), as these make use of radiance ratios to estimate Chl.

Other Drivers of the C:Chl Ratio

Light acclimation is only one possible driver of changes in C:Chl. Nutrient status, phytoplankton community composition and temperature can also affect the C:Chl ratio (e.g., Geider et al., 1998). In an analysis of 10 years of satellite data, Westberry et al. (2016) found an increase in C$_{phyto}$:Chl in summer for both the subarctic North Pacific and North Atlantic oceans. A large part of this increase could be attributed to light acclimation, i.e., increased Chl production in winter. However, these authors also found an influence of nutrient status, especially in the seasonally iron-limited subarctic North Pacific, where increased C:Chl ratios were observed with inferred Fe limitation (Westberry et al., 2016), consistent with results from laboratory studies (Greene et al., 1992; Sunda and Huntsman, 1997). Similarly, in a climatological analysis of cruise data from the Ross Sea, Smith and Kaufman (2018) observed a steady increase in average POC:Chl (weight:weight) from ~90 to 224 from November to

FIGURE 8 | Available mooring data from the SOTS site for **(A)** daily median sea surface temperature, **(B)** salinity and **(C)** daily median mixed layer depth (MLD), estimated based on a temperature threshold of 0.3°C. Gray line indicates a very smoothed GAM for the data to indicate an "average" annual cycle.

February for the shelf region, driven by an increase in POC on a background of variable Chl that peaked in spring and then remained relatively stable. In the context of other data available to them, they interpreted this trend as a shift in community composition from mainly haptophytes, especially *Phaeocystis antarctica*, to diatoms that were increasingly iron-limited (Smith and Kaufman, 2018). Another study, evaluating underway data from several research voyages in the subarctic North Pacific, found that in addition to light acclimation, nitrogen limitation could also be responsible for increased C_{phyto}:Chl ratios (Burt et al., 2018).

Given the development of mixed layer depths over the season at SOTS (**Figure 8**), it is unlikely that nutrient stress can explain the increased $C_{phyto\_b_{bp}}$:Chl-F ratios observed at SOTS in winter. The deep mixed layers observed in winter are likely to represent an injection of nutrients, especially iron, and thus a decrease in the C:Chl ratio would be expected.

In addition to nutrient stress, other possible controls on the C:Chl ratio include phytoplankton seasonal changes in community composition and seasonal changes in the relative contributors to the POC pool such as detritus, bacteria and zooplankton. Large phytoplankton generally show lower C:Chl ratios than small phytoplankton. For example, Sathyendranath et al. (2009) found C:Chl ratios between 15 and 75 for diatoms, while cyanobacteria were in the range 74–126. A progression in community composition from large phytoplankton in summer to small phytoplankton in winter could thus explain at least part of the seasonal signal observed at SOTS. However, microscopic analysis of the phytoplankton community composition between September and April in 2010/2011 did not indicate seasonal dominance by any distinct phytoplankton taxon or size class over the growing season (Eriksen et al., 2018). Rather, the community was diverse throughout the time period sampled (which excluded winter), with a mix of diatoms, haptophytes, nano-, and dino-flagellates as well as ciliates present at all times.

We thus conclude that neither photo-acclimation nor nutrient limitation or changes in community composition can explain the observed seasonal evolution of the C:Chl ratio at SOTS. This prompts the question whether the relative contribution of phytoplankton to the observed b_{bp} signal (and thus to estimated POC) at SOTS is constant over the seasonal cycle. Interpretation of a C:Chl ratio based on b_{bp} is only valid if this assumption holds. Discussing their glider observations in the SAZ, Thomalla et al. (2017) speculate that later in the growing season, a greater percentage of the b_{bp} signal may stem from non-phytoplankton carbon including heterotrophic bacteria, detritus and ciliates. A similar progression can be imagined at SOTS and could explain the observed high C:Chl ratios in winter.

Are We Even Looking at Phytoplankton?

Figure 6 shows that in winter, the observed POC_b_{bp}:Chl-F ratios largely fall outside the bounds of values expected for phytoplankton, regardless of which calibration is used for POC (gray box in **Figures 6A,B**). Two upper bounds were set: 150 g C:g Chl based on POC:Chl values reported by Sathyendranath et al. (2009) for field data spanning two orders of magnitude in Chl concentrations and a variety of dominant phytoplankton taxa

(their Table 4), and 250 g C:g Chl based on the data presented by Taylor et al. (1997) for the North Atlantic, where C refers to "autotrophic carbon" derived from a combination of flow cytometry and epifluorescence microscopy.

Our finding that POC_b_{bp}:Chl-F ratios at SOTS in winter lie outside the limits of what would be expected for phytoplankton could thus suggest that POC components other than phytoplankton may be important contributors to the carbon pool in the SAZ in winter. This would mean that our second hypothesis, expecting that ecosystem structure (trophodynamics) is the dominant driver of the bio-optical signature, might apply. The idea would be that a larger proportion of detritus and non-autotrophic cells is present in winter than in summer, while phytoplankton dominate in summer. Increased POC (and b_{bp}) and less Chl-F (and FChl) would thus be expected in winter.

We explore this contention further by examining the $C_{phyto\_b_{bp}}$:Chl-F relationship (**Figure 7**), where we find that for all but the winter months the estimated C:Chl ratios fall within expected phytoplankton limits as shown by the two gray boxes. The absolute values of our observed $C_{phyto\_b_{bp}}$:Chl-F ratios compare well with C:Chl ratios reported for the Southern Ocean, which tend to fall between 50 and 200 gC:gChl for POC and C_{phyto} estimates based on backscatter in the ocean (Haentjens et al., 2017; Thomalla et al., 2017). Similarly, our data agree well with proxy observations from the subarctic North Pacific and North Atlantic, where ratios between 100 and 300 have been reported, with the majority of values < 100, consistent with our results (Westberry et al., 2016; Burt et al., 2018). This suggests that phytoplankton dominate the particulate carbon pool at SOTS for most of the year, while their role is less prominent in the winter months. To illustrate this point further, the right-hand axes of **Figure 6A** shows the proportion of phytoplankton carbon, f_{phyto}, relative to "other" carbon when a very conservative POC:Chl-F ratio of 200 is assumed for phytoplankton. In the middle of winter, phytoplankton carbon can account for as little as 20% of total carbon.

This is a conservative result, even with the caveat that we may underestimate Chl-F in winter (see section "Potential Seasonal Biases of Calibrations"), which would exaggerate the signal but is unlikely to account for its full magnitude. Even if we assumed the extreme limits of all uncertainties, i.e., a phytoplankton POC:Chl-F ratio of 200, and an underestimation of Chl-F by a factor 10 in winter, some of the observed POC:Chl-F ratios observed at SOTS would still fall outside the phytoplankton envelope (**Figures 6A,B**). The data thus indicate that at SOTS, the relative contribution of non-phytoplankton POC to the backscatter signal increases in the winter months.

Decoupling of the backscatter signal from Chl has been observed in other oceanic regions. For example, Antoine et al. (2011) examined b_{bp}-Chl relationships at the Boussole mooring in the Mediterranean Sea and found that b_{bp} can vary by a factor 5 for Chl concentrations between 0.3 and 1 mg m^{-3} (note that this is extracted Chl, not Chl-F). They interpreted roughly constant backscatter signals at decreasing Chl concentrations as indicating the presence of detritus. Similar to our observations at SOTS, they also found that in spring, after deep winter mixing, Chl

increased much more steeply than b_{bp} (Antoine et al., 2011). At ~1 mg m^{-3} Chl, this signal was followed by b_{bp} going up faster than Chl. Their interpretation was that the initial decoupling of b_{bp} and Chl was the result of chlorophyll synthesis, followed by an increase in phytoplankton biomass. They concluded that "bio-optical relationships might be described as a succession of distinct regimes with rapid transitions among states" (Antoine et al., 2011). Although lacking the temporal component, data from the Atlantic Ocean also indicate that at very low Chl concentrations (below 0.1 mg m^{-3}), b_{bp} and POC remain more or less constant as Chl decreases further (Siegel et al., 2005; Rasse et al., 2017), and the signal is also discernible in global satellite data (Behrenfeld et al., 2005).

At SOTS we observe a very slow increase in POC_b_{bp} between July and September, while Chl-F shows a strong increase of factor ~5 during that time, i.e., after the winter minimum in early July (**Figures 6C,D**). This signal is even more evident in the steep decrease in POC_b_{bp}:Chl-F after the winter peak (**Figure 6A**), followed by a more gradual trend starting in September. Applying the Boussole interpretation to the SOTS data, this would indicate that Chl production in late winter precedes the onset of biomass increase in spring (Antoine et al., 2011). It also indicates that from a bio-optical perspective the winter regime is distinctly different from the regime at other times of the year.

Can an Optical Index Differentiate Between Trophodynamic States of the System?

A number of recent publications have introduced an optical index based on the FChl:b_{bp} ratio designed to trace changes in phytoplankton community composition, especially the rise of diatoms in North Atlantic phytoplankton blooms (e.g., Cetinic et al., 2015; Lacour et al., 2017). The situation at SOTS is arguably different, with peak biomass well below that in the North Atlantic, and also no strong dominance of diatoms during any specific phase of the bloom (Eriksen et al., 2018). Nonetheless, we thought it worthwhile asking whether the FChl:b_{bp} ratio, which doesn't suffer from any uncertainties regarding calibrations (i.e., to convert the bio-optical signal to Chl or carbon), shows a signal that can be interpreted with respect to the trophodynamic shift observed at SOTS over the course of the year.

As seen in **Figure 9**, both FChl and b_{bp} at SOTS show a clear seasonal trend with increases in these properties in austral summer (December-February) and minima in winter. The signal is much more pronounced in FChl, with seasonal variation in the GAM-smoothed signal spanning more than an order of magnitude, while b_{bp} only varies by about a factor 3. There is considerable year-to-year variability in the absolute magnitude of the respective variables, but the overall seasonal trend is consistent in all years. The optical observations are in line with increased phytoplankton productivity in summer, reflected in higher FChl and particle concentrations (b_{bp}) in the water column.
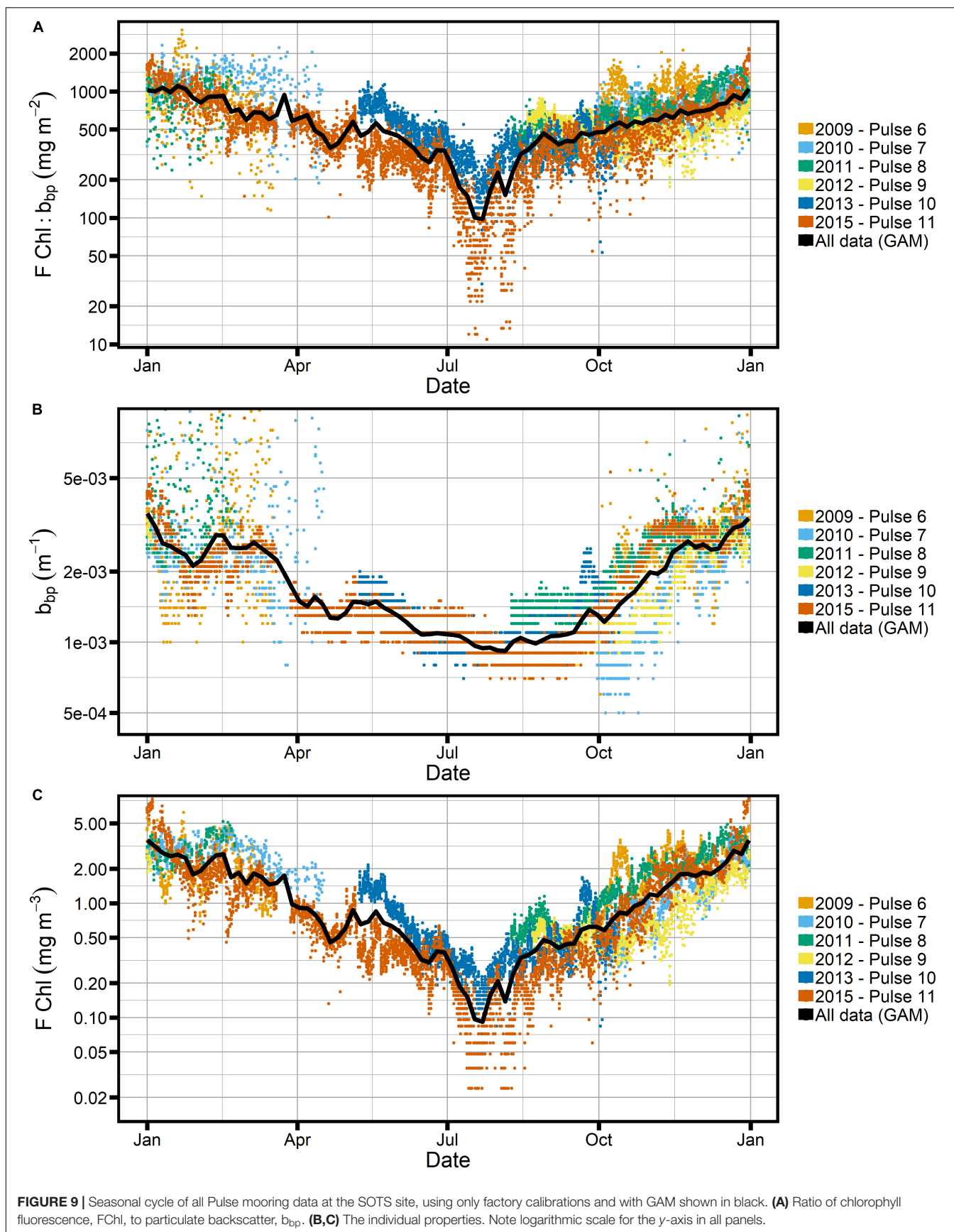
The FChl:b_{bp} ratio follows the same seasonal trend as the individual properties, with increased FChl:b_{bp} in summer relative to winter. It is clear both from the shape of the GAM-smoothed

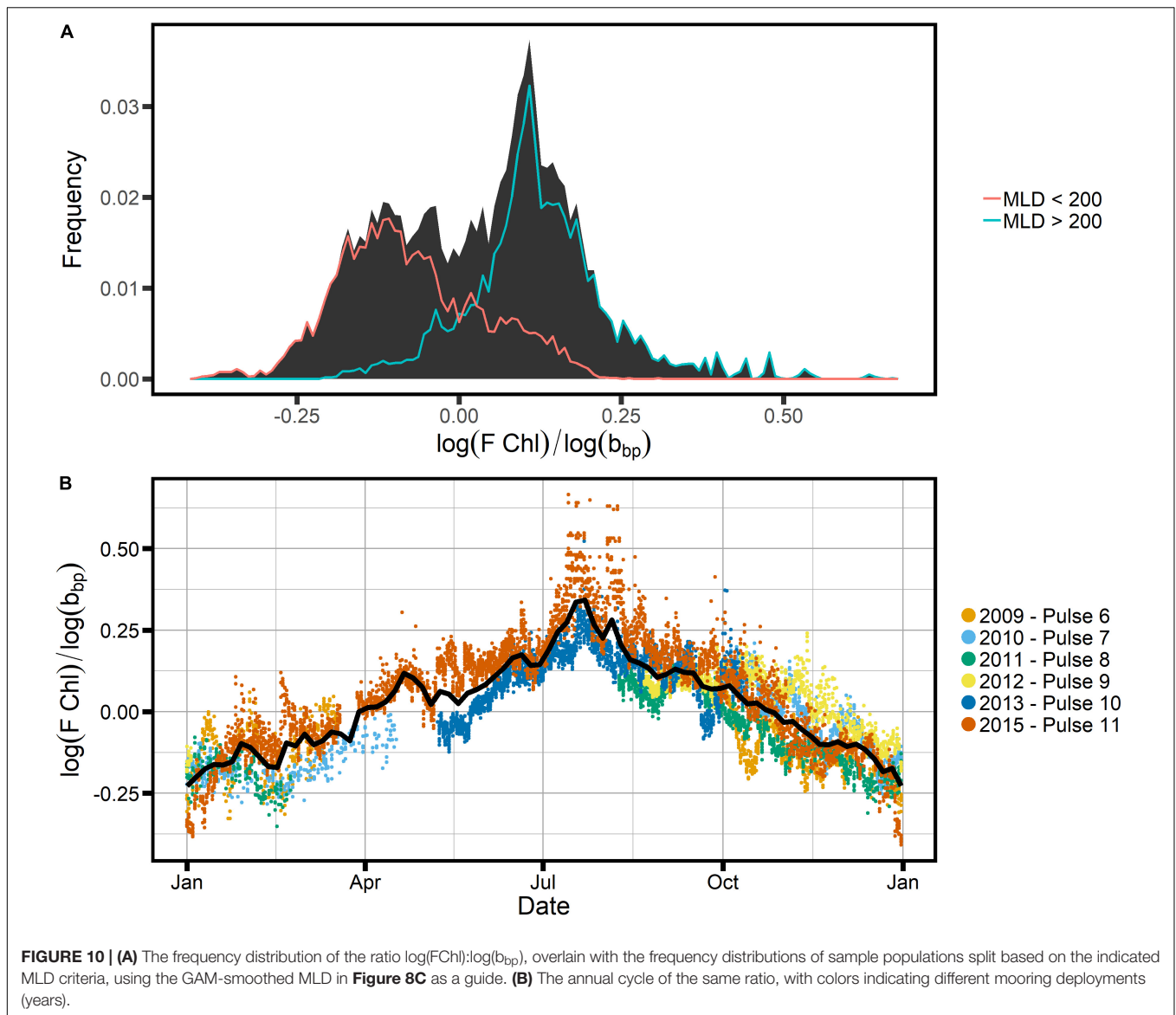seasonal time series of FChl:b_{bp} and from consideration of the absolute seasonal variation in b_{bp} and FChl that the signal is primarily driven by FChl. There is a pronounced "dip" in both FChl and the FChl:b_{bp} ratio in winter, with a minimum in late July. Not surprisingly, the "dip" corresponds with the peak in C:Chl ratios as estimated using both POC_b_{bp} and C$_{phyto}$_b_{bp} (**Figures 6, 7**).

In order to investigate whether the FChl:b_{bp} index shows a clear distinction between the summer and winter communities at SOTS, we plotted the frequency distribution of log(FChl)/log(b_{bp}) (**Figure 10**). We chose the log of the respective entities because both Chl and b_{bp} have log-normal distributions in the ocean (Campbell, 1995). **Figure 10** clearly indicates that two groups can be distinguished: one with a peak around −0.13, and one with a peak around 0.12 (**Figure 10A**). These two groups are indicative of two regimes, one where non-algal particles such as detritus play a significant role, and one where phytoplankton dominate. It appears that the two regimes broadly correspond to changes in the mixed layer, which would indicate that light is a controlling factor: the winter regime begins in late May when mixed layer depths exceed ~200 m (**Figure 8**) and the summer regime begins once the mixed layer shoals to less than ~200 m around the beginning of November. This suggests that the light regime dictates the trophodynamic shift from a phytoplankton-dominated community to one where phytoplankton play a lesser role in the POC pool, as indicated by the C:Chl ratios as well as the FChl:b_{bp} index. We therefore conclude that the FChl:b_{bp} index is a useful indicator of trophodynamics at SOTS but reject the third hypothesis, which proposed that the FChl:b_{bp} ratio at SOTS was driven by floristic shifts in the phytoplankton community.

Other researchers have used the FChl:b_{bp} ratio as a phytoplankton community index, for example indicating diatom dominance at the height of the North Atlantic bloom (e.g., Cetinic et al., 2015). Higher FChl:b_{bp} was observed when diatoms were dominant, while the "recycling community" after the end of the bloom showed lower FChl:b_{bp} (Cetinic et al., 2015). At SOTS, a dominance of diatoms is not expected at any time; instead, a diverse phytoplankton community is present throughout the growing season (Eriksen et al., 2018). This is consistent with the frequency distribution of the FChl:b_{bp} index showing only one distinct group during the growing season, i.e., the time when mixed layers are shallower than 200 m (early November to late May, **Figures 8, 10**).

It is worth noting that the seasonal FChl:b_{bp} trend at SOTS is contrary to Southern Ocean float observations by Barbieux et al. (2018). They found decreased b_{bp}/FChl (which translates to increased FChl:b_{bp}) in winter for the Indian and Atlantic Southern Ocean regions (their **Figure 6**). The source of this discrepancy is unclear; the lack of diatom dominance at SOTS compared to Southern Ocean waters south of the Subantarctic Front could be one possible explanation (e.g., Mendes et al., 2015); the non-photochemical quenching correction on the fluorescence data that was applied by Barbieux et al. (2018) could also have skewed the results, although this seems likely to be a secondary effect given that comparison of non-photochemical quenching corrected and night-time data

FIGURE 9 | Seasonal cycle of all Pulse mooring data at the SOTS site, using only factory calibrations and with GAM shown in black. (A) Ratio of chlorophyll fluorescence, FChl, to particulate backscatter, b_{bp}. (B,C) The individual properties. Note logarithmic scale for the y-axis in all panels.

FIGURE 10 | (A) The frequency distribution of the ratio log(FChl):log(b_{bp}), overlain with the frequency distributions of sample populations split based on the indicated MLD criteria, using the GAM-smoothed MLD in **Figure 8C** as a guide. **(B)** The annual cycle of the same ratio, with colors indicating different mooring deployments (years).

showed good agreement for profiling floats in the biomass-rich iron-fertilized waters downstream from the Kerguelen plateau (Grenier et al., 2015). We further note that our results broadly agree with the conceptual model proposed by Barbieux et al. (2018) for subpolar regimes (their **Figure 8**), although we interpret the shift between summer and winter to be trophodynamic rather than floristic (see above).

Something Happens in July

Both the FChl:b_{bp} index and the respective measures of the C:Chl ratio (**Figures 6**, **7**) show the greatest rate of change around the month of July. The steep increase in FChl:b_{bp} in early August, driven by the increase in FChl, marks the beginning of the transition from one trophodynamic state to the other. As discussed earlier, this increase in FChl on a relatively stable background of b_{bp} (**Figures 9B,C**) likely indicates the synthesis of Chl prior to an increase in phytoplankton biomass. Given that

the mixed layer doesn't begin to shoal until later in the year, this warrants the question why Chl synthesis begins already in July.

Several studies have concluded that the SAZ, in particular the SOTS area, is iron-limited in summer (Sedwick et al., 1999; Boyd et al., 2001; Hutchins et al., 2001; Lannuzel et al., 2011). While Ekman transport from the south has been identified as an important mechanism restoring iron concentrations in the SAZ in winter (Ellwood et al., 2008), deepening of the mixed layer, especially when mixing reaches the ferricline, is also a likely contributor (Tagliabue et al., 2014). It is thus possible that sufficiently deep mixing (e.g., >300 m as seen in July, see **Figure 8**) initiates the transition from iron limiting to iron replete conditions in the SAZ. Given the link between iron availability and chlorophyll synthesis (Greene et al., 1992; Sunda and Huntsman, 1997) and the extreme light limitation expected due to the deep mixed layers, this transition may prompt Chl synthesis in July.

The probable picture that emerges for phytoplankton seasonal dynamics at SOTS is as follows: phytoplankton biomass increases in spring after injection of iron from deep winter mixing and when light limitation is alleviated by a shoaling mixed layer. Later in summer iron limitation coupled with silicate limitation constrains phytoplankton growth (Hutchins et al., 2001). With deepening mixed layers in fall, iron limitation is compounded by light limitation, making SOTS a less favorable environment for phytoplankton, hence the trophodynamic shift away from phytoplankton dominance. When the mixed layer deepens enough to dip into the ferricline, iron limitation is alleviated while light limitation still persists. This leads to an increase in Chl synthesis in winter, but the regime shift to a dominance of phytoplankton is observed only when the mixed layer shoals sufficiently to alleviate light limitation, i.e., in spring. This is consistent with observations from both the Southern Ocean and other oceanic regions such as the North Atlantic, where deep mixed layers in winter do not preclude formation of transient shallower mixing layers, resulting in transient accumulations of Chl at the surface, but the onset of the spring bloom is delayed until the mixed layer shallows sufficiently to allow for net phytoplankton accumulation (Behrenfeld and Boss, 2014; Lacour et al., 2017; Carranza et al., 2018).

The prominent role of the mixed layer in this scenario could also explain the observed differences in the seasonal cycle of the C:Chl ratio between the subarctic Northeast Pacific and the SAZ, with the former showing a strong light-acclimation signature in winter (Westberry et al., 2016). While both areas are seasonally iron-limited, they differ greatly in the annual cycle of their respective C:Chl ratios and mixed layer depths. Due to a permanent halocline, mixed layers in the Northeast Pacific rarely exceed 120 m (Ohno et al., 2004). Given sufficient iron (from either upwelling, lateral transport or atmospheric deposition), increased light limitation in winter can thus be met by increased Chl production, making this region a viable habitat for phytoplankton throughout the year and thus a light-acclimation signal is evident in the annual cycle for the C:Chl ratio (Westberry et al., 2016). In the SAZ, the combination of iron limitation and deepening mixed layers that don't reach the ferricline until late in winter creates an unfavorable environment for phytoplankton, thus the trophodynamic shift away from autotrophy in fall.

Phytoplankton Abundance and Production

The observed seasonality in the evolution of phytoplankton and non-autotrophic carbon broadly agrees with previous findings for the SOTS site within the respective uncertainties. Examining sea surface CO_2 records at SOTS for one yearly cycle, Shadwick et al. (2015) found the mixed layer autotrophic season to last from December through June and the heterotrophic season from July to November. An analysis of nitrogen and oxygen records at the site found NCP in the mixed layer to occur mainly between September and December, but this record did not contain any winter data from before September (Weeding and Trull, 2014). A more recent study using similar methods but including winter

data found that mixed layer NCP is similar in winter and summer at the SOTS site, with a maximum in spring (Trull et al., 2019). All of these estimates are based on gas budgets and suffer from uncertainties related to entrainment during winter. It is thus possible that the results from our study can be reconciled with these respective mixed layer NCP estimates simply by accounting for the uncertainties. However, the slight mismatch between the heterotrophic and autotrophic season identified by Shadwick et al. (2015) and the transitions from one trophic state to another identified in our data could also indicate that the relative abundance of autotrophs relative to heterotrophs and detritus is decoupled from mixed layer NCP. In other words, the relative importance of processes does not mirror relative abundance as estimated by optical methods, i.e., an increase in non-autotrophic POC relative to phytoplankton may not necessarily translate to an equal increase in respiration relative to photosynthesis.

CONCLUSION

The presented analysis of the fluorescence and backscatter records from SOTS has shed new light on the system in several ways. Both the FChl:b_{bp} optical index and the derived C:Chl ratio indicate that the there is a clear distinction between the summer and winter microplankton community. While the summer community is dominated by autotrophs, the winter community appears to consist of an increased proportion of non-phytoplankton carbon. The transition from one community to the other is likely coupled to the evolution of the mixed layer, implicating light limitation as a likely driver. However, acclimation to low light in winter is not evident in the observed C:Chl ratios. This is most likely due to the signal being overwhelmed by the increased proportion of non-autotrophic carbon present in winter, with an additional role of iron limitation hampering Chl synthesis until late in winter, when deep mixing reaches the ferricline.

The optical index has proven to hold valuable information about the trophodynamics at SOTS, indicating two different regimes that present a winter and summer community. However, the signal cannot be interpreted in terms of floristics at the site, due to the lack of a strong dominance by any particular phytoplankton group.

This analysis could be improved with an independent estimator of Chl that does not suffer from the uncertainties associated with chlorophyll fluorescence, e.g., based on radiometers (reflectance ratios) and/or the diffuse light attenuation coefficient. Indeed, the combination of fluorescence with such an independent Chl estimator might provide insights that can only be hinted at in our present analysis, such as the evolution (and possibly episodic relief) of iron limitation at SOTS. Importantly, the presented study provides a baseline to which future time series records at the SOTS site can be compared. For example, southward transport of the East Australian Current is increasing (Hill et al., 2008), and may have growing influence in the SAZ. Bio-optical monitoring tools offer an important path to assess the effects these oligotrophic waters will have on the SAZ ecosystem.

DATA AVAILABILITY STATEMENT

AUTHOR CONTRIBUTIONS

TT and CS conceived the study and developed it further in discussions with JH and PJ. PJ was the SOTS project managing engineer for the moorings construction and deployment, and processed all the ocean sensor records. JH did the data analysis and visualization. DD processed the POC samples from the SAZ-Sense voyage. CS wrote the majority of the manuscript. All authors reviewed and approved the manuscript.

FUNDING

ACKNOWLEDGMENTS

REFERENCES

Ahn, Y. H., Bricaud, A., and Morel, A. (1992). Light backscattering efficiency and related properties of some phytoplankters. *Deep Sea Res.* 39, 1835–1855. doi: 10.1016/0198-0149(92)90002-B

Antoine, D., Siegel, D. A., Kostadinov, T., Maritorena, S., Nelson, N. B., Gentili, B., et al. (2011). Variability in optical particle backscattering in contrasting bio-optical oceanic regimes. *Limnol. Oceanogr.* 56, 955–973. doi: 10.4319/lo.2011.56.3.0955

Barbieux, M., Uitz, J., Bricaud, A., Organelli, E., Poteau, A., and Schmechtig, C. (2018). Assessing the variability in the relationship between the particulate backscattering coefficient and the chlorophyll a concentration from a global Biogeochemical-Argo database. *J. Geophys. Res. Oceans* 123, 1229–1250. doi: 10.1002/2017jc013030

Behrenfeld, M. J., Boss, E., Siegel, D. A., and Shea, D. M. (2005). Carbon-based ocean productivity and phytoplankton physiology from space. *Global Biogeochem. Cycles* 19:GB1006. doi: 10.1029/2004GB002299

Behrenfeld, M. J., and Boss, E. S. (2014). Resurrecting the ecological underpinnings of ocean plankton blooms. *Annu. Rev. Mar. Sci.* 6, 167–194. doi: 10.1146/annurev-marine-052913-021325

Behrenfeld, M. J., Westberry, T. K., Boss, E. S., O'Malley, R. T., Siegel, D. A., and Wiggert, J. D. (2009). Satellite-detected fluorescence reveals global physiology of ocean phytoplankton. *Biogeosciences* 6, 779–794. doi: 10.5194/bg-6-779-2009

Bellido, J. M., Pierce, G. J., and Wang, J. (2001). Modelling intra-annual variation in abundance of squid loligo forbesi in scottish waters using generalised additive models. *Fish. Res.* 52, 23–39. doi: 10.1016/s0165-7836(01)00228-4

Bowie, A. R., Griffiths, B., Dehairs, F., and Trull, T. W. (2011a). Oceanography of the subantarctic and polar frontal zones south of Australia during summer: setting for the SAZ-Sense study. *Deep Sea Res. II* 58, 2059–2070. doi: 10.1016/j.dsr2.2011.05.033

Bowie, A. R., Trull, T. W., and Dehairs, F. (2011b). Estimating the sensitivity of the subantarctic zone to environmental change: the SAZ-Sense project. *Deep Sea Res. II* 58, 2051–2058. doi: 10.1016/j.dsr2.2011.05.034

Bowie, A. R., Lannuzel, D., Remenyi, T. A., Wagener, T., Lam, P. J., Boyd, P. W., et al. (2009). Biogeochemical iron budgets of the southern ocean south of Australia: decoupling of iron and nutrient cycles in the subantarctic zone by the summertime supply. *Global Biogeochem. Cycles* 23:GB4034. doi: 10.1029/2009GB003500

Boyd, P. W., Crossley, A. C., DiTullio, G. R., Griffiths, F. B., Hutchins, D. A., Queguiner, B., et al. (2001). Control of phytoplankton growth by iron supply and irradiance experimental results from the SAZ project chlorophyll a levels increased experiment there were increases in chlorophyll. *J. Geophys. Res.* 106, 31573–31583. doi: 10.1029/2000jc000348

Burt, W., Westberry, T., Behrenfeld, M., Zeng, C., Izett, R. W., and Tortell, P. (2018). Carbon:Chlorophyll ratios and net primary productivity of subarctic Pacific surface waters derived from autnonomous shipboard sensors. *Global Biogeochem. Cycles.* 32, 267–288. doi: 10.1002/2017GB005783

Campbell, J. (1995). The lognormal distribution as a model for bio-optical variability in the sea. *J. Geophys. Res.* 100, 13237–13254.

Carranza, M. M., Gille, S. T., Franks, P. J. S., Johnson, K. S., Pinkel, R., and Girton, J. B. (2018). When mixed layers are not mixed. storm-driven mixing and bio-optical vertical gradients in mixed layers of the Southern Ocean. *J. Geophys. Res. Oceans* 123, 7264–7289. doi: 10.1029/2018jc014416

Cassar, N., Wright, S., Thomson, P., Trull, T., Westwood, K., and de Salas, M. (2015). The relation of mixed-layer net community production to phytoplankton community composition in the Southern Ocean. *Global Biogeochem. Cycles* 29, 446–462. doi: 10.1002/2014GB004936

Cetinic, I., Perry, M. J., Asaro, E. D., Briggs, N., Poulton, N., and Sieracki, M. E. (2015). A simple optical index shows spatial and temporal heterogeneity in phytoplankton community composition during the 2008 North Atlantic bloom experiment. *Biogeosciences* 12, 2179–2194. doi: 10.5194/bg-12-2179-2015

Cetinic, I., Perry, M. J., Briggs, N. T., Kallin, E., D'Asaro, E. A., and Lee, C. M. (2012). Particulate organic carbon and inherent optical properties during 2008 North Atlantic bloom experiment. *J. Geophys. Res.* 117:C06028. doi: 10.1029/2011JC007771

Cullen, J. J., and Lewis, M. R. (1995). Biological processes and optical measurements near the sea surface: some issues relevant to remote sensing. *J. Geophys. Res.* 100, 13255–13266. doi: 10.1029/95jc00454

de Salas, M. F., Eriksen, R., Davidson, A. T., and Wright, S. W. (2011). Protistan communities in the Australian sector of the sub-antarctic zone during SAZ-Sense. *Deep Sea Res. II* 58, 2135–2149. doi: 10.1016/j.dsr2.2011.05.032

Ellwood, M. J., Boyd, P. W., and Sutton, P. (2008). Winter-time dissolved iron and nutrient distributions in the subantarctic zone from 40 – 52S; 155 – 160E. *Geophys. Res. Lett.* 35 1–6. doi: 10.1029/2008GL033699

Eriksen, R., Trull, T. W., Davies, D., Jansen, P., Davidson, A. T., Westwood, K., et al. (2018). Seasonal succession of phytoplankton community structure from autonomous sampling at the Australian southern ocean time series (SOTS) observatory. *Mar. Ecol. Prog. Ser.* 589, 13–31. doi: 10.3354/meps12420

Falkowski, P. G., and LaRoche, J. (1991). Acclimation to spectral irradiance in algae. *J. Phycol.* 27, 8–14. doi: 10.1111/j.0022-3646.1991.00008.x

Geider, R. J. (1987). Light and temperature dependence of the carbon to chlorophyll a ratio in microalgae and cyanobacteria: implications for physiology and growth of phytoplankton. *New Phytol.* 106, 1–34. doi: 10.1111/j.1469-8137.1987.tb04788.x

Geider, R. J., MacIntyre, H. L., and Kana, T. M. (1998). A dynamic regulatory model of phytoplanktonic acclimation to light, nutrients and temperature. *Limnol. Oceanogr.* 43, 679–694. doi: 10.4319/lo.1998.43.4.0679

Graff, J. R., Westberry, T. K., Milligan, A. J., Brown, M. B., Dall'Olmo, G., and Reifel, K. M. (2016). Photoacclimation of natural phytoplankton communities. *Mar. Ecol. Prog. Ser.* 542, 51–62. doi: 10.3354/meps11539

Graff, J. R., Westberry, T. K., Milligan, A. J., Brown, M. B., Dall'Olmo, G., and van Dongen-Vogels, V. (2015). Phytoplankton carbon measurements spanning diverse ecosystems. *Deep Sea Res. I* 102, 16–25. doi: 10.1016/j.dsr.2015.04.006

Greene, R. M., Geider, R. J., Kolber, Z., and Falkowski, P. G. (1992). Iron-induced changes in light harvesting and photochemical energy conversion processes in eukaryotic marine algae '. *Plant Physiol.* 100, 565–575. doi: 10.1104/pp.100.2.565

Grenier, M., Della Penna, A., and Trull, T. W. (2015). Autonomous profiling float observations of the high-biomass plume downstream of the kerguelen plateau in the Southern Ocean. *Biogeosciences* 12, 2707–2735. doi: 10.5194/bg-12-2707-2015

Haentjens, N., Boss, E., and Talley, L. (2017). Revisiting Ocean Color algorithms for chlorophyll a and particulate organic carbon in the Southern Ocean using biogeochemical floats. *J. Geophys. Res. Oceans* 122, 6583–6593. doi: 10.1002/2017JC012844

Herraiz-Borreguero, L., and Rintoul, S. R. (2011). Regional circulation and its impact on upper ocean variability south of Tasmania. *Deep Sea Res. II* 58, 2071–2081. doi: 10.1016/j.dsr2.2011.05.022

Hill, K. L., Rintoul, S. R., Coleman, R., and Ridgway, K. R. (2008). Wind forced low frequency variability of the east Australia current. *Geophys. Res. Lett.* 35, 1–5. doi: 10.1029/2007GL032912

Hutchins, D. A., Sedwick, P. N., DiTullio, G. R., Boyd, P. W., Queguiner, B., Griffiths, F. B., et al. (2001). Control of phytoplankton growth by iron and silicic acid availability in the subantarctic southern ocean: experimental results from the SAZ Project with or without. *J. Geophys. Res.* 106, 31559–31572. doi: 10.1029/2000jc000333

Lacour, L., Ardyna, M., Stec, K. F., Claustre, H., Prieur, L., Poteau, A., et al. (2017). Unexpected winter phytoplankton blooms in the North Atlantic subpolar gyre. *Nat. Geosci.* 10, 836–839. doi: 10.1038/NGEO3035

Lannuzel, D., Bowie, A. R., Remenyi, T., Lam, P., Townsend, A., and Ibisanmi, E. (2011). Distributions of dissolved and particulate iron in the sub-Antarctic and Polar Frontal Southern Ocean (Australian sector). *Deep Sea Res. II* 58, 2094–2112. doi: 10.1016/j.dsr2.2011.05.027

Longhurst, A. R. (2007). *Ecological Geography of the Sea.* Amsterdam: Elsevier.

Lorenzen, C. (1966). A method for the continuous measurement of in vivo chlorophyll concentration. *Deep Sea Res.* 13, 223–227. doi: 10.1038/421028a

Lourey, M., and Trull, T. (2001). Seasonal nutrient depletion and carbon export in the Subantarctic and Polar Frontal Zones of the Southern Ocean south of Australia. *Geophys. Res. Oceans* 106 31463–31487. doi: 10.1029/2000jc000287

Maronna, R. A., and Yohai, V. J. (2000). Robust regression with both continuous and categorical predictors. *J. Statist. Plan. Inference* 89, 197–214. doi: 10.1016/s0378-3758(99)00208-6

Mendes, C. R. B., Kerr, R., Tavano, V. M., Carvalheiro, F. A., Garcia, C. A. E., and Dessai, D. R. G. (2015). Cross-front phytoplankton pigments and chemotaxonomic groups in the Indian sector of the Southern Ocean. *Deep Sea Res. II* 118, 221–232. doi: 10.1016/j.dsr2.2015.01.003

Mongin, M., Matear, R., and Chamberlain, M. (2011). Seasonal and spatial variability of remotely sensed chlorophyll and physical fields in the SAZ-Sense region. *Deep Sea Res. Part II Topical Stud. Oceanogr.* 58, 2082–2093. doi: 10.1016/j.dsr2.2011.06.002

Morel, A., and Ahn, Y.-H. (1991). Optics of heterotrophic nanoflagellates and ciliates: a tentative assessment of their scattering role in oceanic waters compared to those of bacterial and algal cells. *J. Mar. Res.* 49, 177–202. doi: 10.1357/002224091784698639

Ohno, Y., Kobayashi, T., Iwasaka, N., and Suga, T. (2004). The mixed layer depth in the North Pacific as detected by the Argo floats. *Geophys. Res. Lett.* 31, L11306. doi: 10.1029/2004GL019576

Organelli, E., Dall'Olmo, G., Brewin, R. J. W., Tarran, G. A., Boss, E., and Bricaud, A. (2018). The open-ocean missing backscattering is in the structural complexity of particles. *Nat. Commun.* 9:5439. doi: 10.1038/s41467-018-07814-6

Proctor, C. W., and Roesler, C. S. (2010). New insights on obtaining phytoplankton concentration and composition from in situ multispectral Chlorophyll fluorescence. *Limnol. Oceanogr. Methods* 8, 695–708. doi: 10.4319/lom.2010.8.695

Rasse, R., Dall'Olmo, G., Graff, J., Westberry, T. K., van Dongen-Vogels, V., and Behrenfeld, M. J. (2017). Evaluating optical proxies of particulate organic carbon across the surface Atlantic Ocean. *Front. Mar. Sci.* 4:367. doi: 10.3389/fmars.2017.00367

Rembauville, M., Briggs, N., Ardyna, M., Uitz, J., Catala, P., and Penkerc'ch, C. (2017). Plankton assemblage estimated with BGC-Argo floats in the Southern Ocean: implications for seasonal successions and particle export. *J. Geophys. Res. Oceans* 122, 8278–8292. doi: 10.1002/2017jc013067

Roesler, C., Uitz, J., Claustre, H., Boss, E., Xing, X., and Organelli, E. (2017). Recommendations for obtaining unbiased chlorophyll estimates from in situ chlorophyll fluorometers: a global analysis of WET Labs ECO sensors. *Limnol. Oceanogr. Methods* 15, 572–585. doi: 10.1002/lom3.10185

Ryan-Keogh, T. J., Thomalla, S. J., Mtshali, T. N., Van Horsten, N. R., and Little, H. J. (2018). Seasonal development of iron limitation in the sub-Antarctic zone. *Biogeosciences* 15, 4647–4660. doi: 10.5194/bg-15-4647-2018

Sarmiento, J. L., Gruber, N., Brzezinski, M. A., and Dunne, J. P. (2004). High-latitude controls of thermocline nutrients and low latitude biological productivity. *Nature* 427, 56–60. doi: 10.1038/nature10605

Sathyendranath, S., Stuart, V., Nair, A., Oka, K., Nakane, T., and Bouman, H. (2009). Carbon-to-chlorophyll ratio and growth rate of phytoplankton in the sea. *Mar. Ecol.Prog. Ser.* 383, 73–84. doi: 10.3354/meps07998

Schallenberg, C., Jansen, P., and Trull, T. (2019). *Southern Ocean Time Series (SOTS) Quality Assessment and Control Report Wetlabs FLNTUS instruments Version 2.0.* Hobart: CSIRO, 37.

Sedwick, P., DiTullio, G., Hutchings, D., Boyd, P., Griffiths, F., Crossley, A. C., et al. (1999). Limitation of algal growth by iron deficiency in the Australian subantarctic region. *Geophys. Res. Lett.* 26, 2865–2868. doi: 10.1029/1998gl002284

Shadwick, E. H., Thomas, H., Azetsu-Scott, K., Greenan, B. J. W., Head, E., and Horne, E. (2011). Seasonal variability of dissolved inorganic carbon and surface water pCO2 in the Scotian Shelf region of the Northwestern Atlantic. *Mar. Chem.* 124, 23–37. doi: 10.1016/j.marchem.2010.11.004

Shadwick, E. H., Trull, T. W., Tilbrook, B., Sutton, A. J., Schulz, E., and Sabine, C. L. (2015). Seasonality of biological and physical controls on surface ocean CO2 from hourly observations at the Southern Ocean time series site south of Australia. *Global Biogeochem. Cycles* 29, 223–238. doi: 10.1002/2014GB004906

Siegel, D. A., Maritorena, S., Nelson, N. B., and Behrenfeld, M. J. (2005). Independence and interdependencies among global ocean color properties: reassessing the bio-optical assumption. *J. Geophys. Res.* 110, 1–14. doi: 10.1029/2004JC002527

Sigman, D. M. D., and Boyle, E. E. A. (2000). Glacial/interglacial variations in atmospheric carbon dioxide. *Nature* 407, 859–869. doi: 10.1038/35038000

Smith, R. C., and Baker, K. S. (1978). The bio-optical state of ocean waters and remote sensing. *Limnol. Oceanogr.* 23, 247–259. doi: 10.4319/lo.1978.23.2.0247

Smith, W. O., and Kaufman, D. E. (2018). Climatological temporal and spatial distributions of nutrients and particulate matter in the Ross Sea. *Progr. Oceanogr.* 168, 182–195. doi: 10.1016/j.pocean.2018.10.003

Stramski, D., and Kiefer, D. A. (1991). Light scattering by microorganisms in the open ocean. *Progr. Oceanogr.* 28, 343–383. doi: 10.1016/0079-6611(91)90032-H

Stramski, D., Reynolds, R. A., Kahru, M., and Mitchell, B. G. (1999). Estimation of particulate organic carbon in the ocean from satellite remote sensing. *Science* 285, 239–242. doi: 10.1126/science.285.5425.239

Sullivan, J., and Twardowski, M. (2009). Angular shape of the oceanic particulate volume scattering function in the backward direction. *Appl. Opt.* 48, 6811–6819. doi: 10.1364/AO.48.006811

Sunda, W., and Huntsman, S. A. (1997). Interrelated influence of iron, light and cell size on marine phytoplankton growth. *Nature* 390, 389–392. doi: 10.1038/37093

Tagliabue, A., Sallée, J., Bowie, A., and Lévy, M. (2014). Surface-water iron supplies in the Southern Ocean sustained by deep winter mixing. *Nat. Geosci.* 7, 314–320. doi: 10.1038/NGEO2101

Taylor, A. H., Geider, R. J., and Gilbert, F. J. H. (1997). Seasonal and latitudinal dependencies of phytoplankton carbon-to-chlorophyll a ratios: results of a modelling study. *Mar. Ecol. Progr. Ser.* 152, 51–66. doi: 10.3354/meps152051

Terrill, E. J., Melville, W. K., and Stramski, D. (2001). Bubble entrainment by breaking waves and their influence on optical scattering in the upper ocean. *J. Geophys. Res.* 106, 16815–16823. doi: 10.1029/2000jc000496

Thomalla, S. J., Ogunkoya, A. G., Vichi, M., and Swart, S. (2017). Using optical sensors on gliders to estimate phytoplankton carbon concentrations and chlorophyll-to-carbon ratios in the Southern Ocean. *Front. Mar. Sci.* 4:34. doi: 10.3389/fmars.2017.00034

Trull, T., Jansen, P., Schulz, E., Weeding, B., Davies, D., and Bray, S. (2019). Autonomous multi-trophic observations of productivity and export at the Australian Southern Ocean Time Series (SOTS) reveal sequential mechanisms of physical-biological coupling. *Front. Mar. Sci.* 6:525. doi: 10.3389/fmars.2019.00525

Trull, T., Schulz, E., Bray, S., Pender, L., McLaughlan, D., Tilbrook, B., et al. (2010). *The Australian Integrated Marine Observing System Southern Ocean Time Series facility.* Sydney: IEEE.

Trull, T. W., Bray, S. G., Manganimi, S. J., Honjo, S., and François, R. (2001). Moored sediment trap measurements of carbon export in the subantarctic and polar frontal zones of the Southern Ocean, south of Australia. *J. Geophys. Res.* 106, 31489–31509. doi: 10.1029/2000jc000308

Underwood, F. M. (2009). Describing long-term trends in precipitation using generalized additive models. *J. Hydrol.* 364, 285–297. doi: 10.1016/j.jhydrol.2008.11.003

Vaillancourt, R. D., Brown, C. W., Guillard, R. R. L., and Balch, W. M. (2004). Light backscattering properties of marine phytoplankton: relationships to cell size, chemical composition and taxonomy. *J. Plankton Res.* 26, 191–212. doi: 10.1093/plankt/fbh012

Vichi, M., Allen, J. I., Masina, S., and Hardman-Mountford, N. J. (2011). The emergence of ocean biogeochemical provinces: a quantitative assessment and a diagnostic for model evaluation. *Global Biogeochem. Cycles* 25:GB2005. doi: 10.1029/2010GB003867

Weeding, B., and Trull, T. W. (2014). Hourly oxygen and total gas tension measurements at the Southern Ocean time series site reveal winter ventilation and spring net community production. *J. Geophys. Res. Oceans* 119, 348–358. doi: 10.1002/2013JC009302

Westberry, T. K., Schultz, P., Behrenfeld, M. J., Dunne, J. P., Hiscock, M. R., and Maritorena, S. (2016). Annual cycles of phytoplankton biomass in the subarctic Atlantic and Pacific Ocean. *Global Biogeochem. Cycles* 30, 175–190. doi: 10.1002/2015GB005276

Whitmire, A. L., Pegau, W. S., Karp-Boss, L., Boss, E., and Cowles, T. J. (2010). Spectral backscattering properties of marine phytoplankton cultures. *Optics Express* 18, 1680–1690. doi: 10.1029/2003RG000148.D

Wood, S. N. (2001). mgcv: GAMs and generalized ridge regression for R. *R news* 1, 20–25.

Xing, X., Claustre, H., Blain, S., D'Ortenzio, F., Antoine, D., Ras, J., et al. (2012). Quenching correction for in vivo chlorophyll fluorescence acquired by autonomous platforms: a case study with instrumented elephant seals in the Kerguelen region (Southern Ocean). *Limnol. Oceanogr. Methods.* 10, 483–495. doi: 10.4319/lom.2012.10.483

Xing, X., Claustre, H., Boss, E. S., Roesler, C., Organelli, E., and Poteau, A. (2016). Correction of profiles of in-situ chlorophyll fluorometry for the contribution of fluorescence originating from non-algal matter. *Limnol. Oceanogr. Methods* 15, 80–93. doi: 10.1002/lom3.10144

Zhang, X., Hu, L., and He, M.-X. (2009). Scattering by pure seawater at high salinity. *Optics Express* 17, 12685–12691. doi: 10.1364/oe.17.012685

Zhang, X., Lewis, M., and Johnson, B. (1998). Influence of bubbles on scattering of light in the ocean. *Appl. Opt.* 37, 6252–6236.

Zhang, X., Twardowski, M., and Lewis, M. (2011). Retrieving composition and sizes of oceanic particle subpopulations from the volume scattering function. *Appl.Opt.* 50, 1240–1259. doi: 10.1364/AO.50.001240